Available online at www.sciencedirect.com

ScienceDirect

Geochimica et Cosmochimica Acta 258 (2019) 97–119

Geochimica et Cosmochimica Acta

www.elsevier.com/locate/gca

A diagenetic origin for isotopic variability of sediments deposited on the margin of Great Bahama Bank, insights from clumped isotopes

Philip T. Staudigel [a,b,*], Peter K. Swart [a]

[a] *Rosenstiel School of Marine and Atmospheric Sciences, Department of Marine Geosciences, University of Miami, Miami FL 33149, United States*

[b] *Cardiff University, School of Earth and Ocean Sciences, United Kingdom*

Received 22 August 2018; accepted in revised form 1 May 2019; Available online 28 May 2019

Abstract

The clumped isotope temperature proxy has been used to investigate the diagenetic history of carbonate sediments in two cores recovered during ODP Leg 166 on the margin of Great Bahama Bank. While periplatform sediments constitute a tempting archive of paleo ocean chemistry as they are unlikely to be subducted, their primary limitation is a well-documented susceptibility to post-depositional diagenetic reworking. The crystallization temperatures reconstructed using the clumped isotope proxy, as well as the mineralogy and $\delta^{13}C$ and $\delta^{18}O$ values have been used to determine the relative effects of sediment mixing and sediment recrystallization. Results show that as sediments undergo diagenetic alteration at the seafloor, their initially "warm" clumped isotope composition is overprinted at cooler benthic temperatures. This process appears to occur in an environment with sufficient fluid exchange to overprint carbon isotopes; an observation confirmed in a separate study by analyses of calcium, a similarly rock-buffered element. This early reactive exchange between carbonates and fluids is likely driven by the conversion of metastable aragonite to calcite. This partially occurs within the "flushed zone", where porewater compositions remain compositionally similar to seawater throughout the upper ~40 meters of the sediment column. Sediments dominated by open system isotopic compositions correspond to a period of minimal sediment accumulation between 2 and 3 Ma. More deeply buried Miocene sediments of the more platform-proximal Site 1003 show evidence of subsequent recrystallization, incorporating the warmer geothermal $T\Delta_{47}$ values, and more as well as modified water $\delta^{18}O$ values, likely driven by co-evolving porewater and carbonate oxygen isotopes. Reconstructed water $\delta^{18}O$ values of these deeper sediments at Site 1003 are considerably more positive than the measured modern values, suggesting that porewater $\delta^{18}O$ values were more positive during the Miocene. Sediments deposited at the platform distal Site 1006 between the early and middle Miocene did not show evidence for this deeper recrystallization. Differences in diagenetic behavior between the two sites cannot be solely accounted for by differences in sediment accumulation rate. To illustrate this, time-integrated models were constructed which simulated the burial of identically reactive material through the depositional history of each site, the sediments deposited at Site 1006 appear to "stabilize" after an initial phase of neomorphism, whereas the more platform proximal Site 1003 continues to recrystallize during deeper burial, apparently in the presence of a parent fluid with a more positive $\delta^{18}O$ value than observed today. We conclude that despite consisting of the same end-member sediment sources, and being spatially separated by less than 30 km, the difference in clumped and oxygen isotopic composition between Sites 1003 and 1006 can be predominantly attributed to differences in the rate and duration of recrystallization during burial.

Keywords: Periplatform sediments; Diagenesis; Clumped isotopes; Water isotope reconstruction; Fluid-rock interaction

* Corresponding author.
E-mail address: staudigelP@cardiff.ac.uk (P.T. Staudigel).

https://doi.org/10.1016/j.gca.2019.05.002
0016-7037/

1. INTRODUCTION

1.1. Periplatform sediments

Sediments deposited adjacent to carbonate platforms, termed periplatform sediments, consist of a variable mixture of platform-derived and pelagic sediments (Boardman and Neumann, 1984; Schlager and James, 1978). Whereas zones of active periplatform sedimentation do not constitute the majority of carbonate deposition at the present time (Taft, 1967), the resulting sediments are more likely to be preserved due to the nearly inevitable subduction of the more abundant pelagic sediments. As a result, periplatform deposits deposited on passive continental margins are comparatively more abundant in the ancient record, and deposits of this nature constitute a valuable geochemical archive of Mesozoic and Paleozoic climate and ocean chemistry (Jones et al., 2015; Skelton and Gili, 2012; van der Kooij et al., 2009).

Investigations of the spatial variance of geochemical proxies such as the $\delta^{13}C$ and $\delta^{18}O$ values of platform-margin sediments have demonstrated that changes in the relative supply of sediment sources (Swart and Eberli, 2005) and variation in diagenetic processes (Immenhauser et al., 2002; van der Kooij et al., 2009) can result in significant differences in synchronously formed sediment.

Modern platform-derived sediment consists predominantly of aragonite, a metastable polymorph of calcium carbonate that readily dissolves and reprecipitates as calcite (Bischoff and Fyfe, 1968; Folk, 1965; Lasemi and Sandberg, 1984). Modern platform sediments on the Great Bahama Bank (GBB) range in grainsize between fine muds, mm-scale peloids, macroalgal carbonate, bryozoans and coral fragments (Purdy, 1963a,b) with $\delta^{13}C$ and $\delta^{18}O$ values ranging between +4.0 and +5.5‰ and −0.5 and 2‰ (VPDB) respectively (Lowenstam and Epstein, 1957; Swart et al., 2009).

As carbonate sediments are buried they undergo a series of transformations in which the original components are dissolved and authigenic minerals, usually low magnesium calcite (LMC) and dolomite are precipitated. If the process taking place does not involve the conversion from one mineral to another, then this is defined as recrystallization (Sorby, 1879; Vaughan and Dixon, 1911); this process usually involves an increase in crystal size within the rock. Conversion of one mineral to another, for example aragonite to LMC, has been termed neomorphism (Folk, 1965). Both processes may occur at the same time in the environments discussed in this manuscript; due to the intimate mixing of these processes, we have used the term recrystallization in this paper to encompass both processes, whereas the term neomorphism is used exclusively to describe the polymorphic transition from aragonite to calcite.

1.2. Site descriptions

This study focuses on two cores recovered by Ocean Drilling Program (ODP) Leg 166 in 1996, Sites 1003 and 1006 (Fig. 1). Leg 166 recovered five cores from the platform margin along the "western seismic line" (shown in Fig. 2), this line extends onto the platform top, where two cores, termed 'Clino' and 'Unda' were collected (Eberli et al., 1997b; Ginsburg, 2001) in 1990. Site 1003 was drilled on the mid-slope of the GBB, recovering over 1.2 km of early Miocene to modern sediments. Site 1006 is the most platform-distal site recovered on Leg 166 sampling 700 m of mid-Miocene to modern sediments (Fig. 2). Sediments deposited near the platform margin of GBB (sampled at Site 1003) consisted predominantly of west-dipping platform-derived sediments which formed predominantly during sea-level high stands and of drift deposits emplaced by benthic currents, shown in Fig. 2 (Anselmetti et al., 2000; Betzler et al., 1999). The sediments recovered at the most distal site (1006) consisted of a mixture of platform and pelagic sediments deposited as drift deposits emplaced by currents in the channel.

The Santaren Channel and Florida Straits feature a temperature gradient, ranging between 20 and 30 °C at the surface to <10 °C at depth (Leaman et al., 1995; Lüdmann et al., 2016). The geothermal gradients at Sites 1003 and 1006 are of 33.1 ± 1.5 °C/km and 36.8 ± 0.1 °C/km respectively (Fig. 3) (Eberli et al, 1997b). Extrapolation of these values to the sea floor at Sites 1003 and 1006 indicate benthic temperatures of 14.9 °C and 8.4 °C, respectively and are in agreement with the values presented by Lüdmann et al. (2016) and Leaman et al. (1995), although the in situ measurements do suggest a slightly cooler benthic temperature for Site 1003 (~13 °C).

Sediments deposited on platform margins experience a range of temperatures from initial precipitation in surface waters, through subsequent deposition and burial. Sediments are initially formed in warm surface waters on the platform top or near the sea surface at temperatures between ~20 and 30 °C (Cloud, 1962; Reijmer et al.,

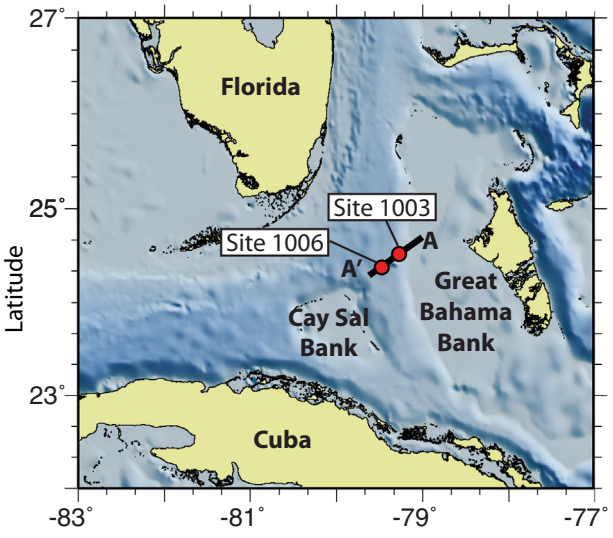

Fig. 1. Location of ODP Sites 1003 and 1006, relative to Florida, the Bahamas and Cuba. "Western Line" seismic profile A–A′ shown in Fig. 2.

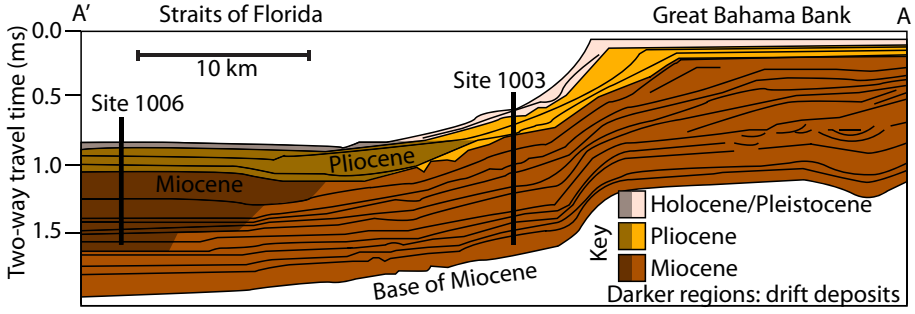

Fig. 2. Seismic cross-section A–A′ from Fig. 1, Sites 1006 and 1003 shown. Sediments colored by age, darker region delineates extent of channel drift deposits. Modified from Eberli et al. (2002).

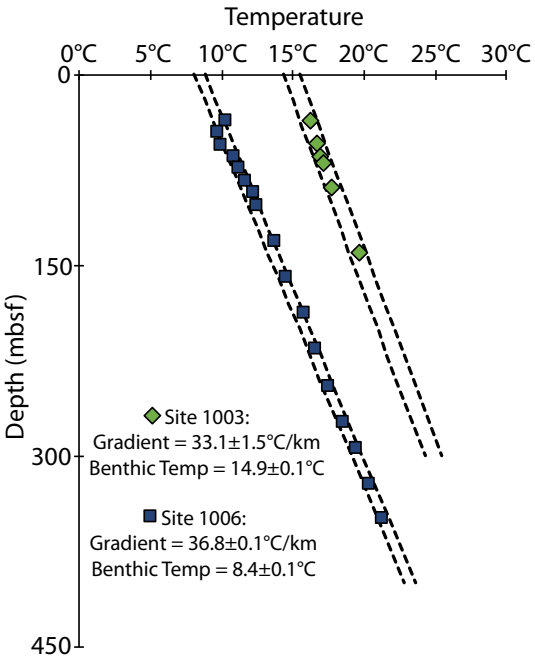

Fig. 3. Downcore temperatures (omitting "anomalous/poor recovery" data) reported by the shipboard scientific party (Eberli et al, 1997b). Plotted uncertainty: ±95% confidence for linear regression.

2009). As they are swept off the platform and are deposited sea floor they experience cooler benthic temperatures. During burial, sediments will gradually increase in temperature due to the geothermal gradient (Fig. 3). As a result of this thermal history, sediments may recrystallize at a variety of temperatures.

1.2.1. Estimating recrystallization rate using porefluid Sr^{2+}/Ca^{2+} ratios

The dissolution of aragonite and precipitation of calcite at equilibrium results in an increase in concentration of Sr^{2+} within the pore fluids, as it is excluded during the precipitation of calcite (Katz et al., 1972). During burial, reactively supplied strontium diffuses upwards along a concentration gradient (Baker et al., 1982), governed by Fick's Law.

$$\mathrm{Flux}(Sr^{2+}) = -D * d[Sr^{2+}]/dz \quad (1)$$

At Sites 1003 and 1006 strontium in the pore water increases in abundance from seawater concentrations of ~90–1300 μM at 200 mbsf and 6300 μM at 425 mbsf respectively. Modeling this gradient over time can provide an estimate of the amount of strontium removed from the sediment, and assuming that there are no other sources or sinks of strontium, the amount of recrystallization can be estimated. Using a diffusion coefficient (D) of 3.5×10^{-6} cm^2/s (Compton and Siever, 1986) a net Sr^{2+} flux of 124 and 181 $mol/cm^2/myr$ can be estimated for Sites 1003 and 1006 respectively, requiring a minimum rate of neomorphism of 2%/myr and 5%/myr over the respective depth intervals. These calculations can only provide a minimum estimate at Site 1003, as sediments quickly reach the saturation state with respect to celestine providing a significant additional sink for strontium (Swart and Guzikowski, 1988). In addition, both sites have evidence for significant advection in the uppermost sediments, which was termed the "flushed zone" by Kramer et al. (2000) and Swart (2000). Site 1006 never reaches celestine saturation as a result of bacterial sulfate reduction and lower rates of recrystallization (Kramer et al., 2000).

1.2.2. Oxygen isotopes in pore fluids

Porewater $\delta^{18}O$ values at Site 1003 increase downcore from the benthic value of ~0.5‰ reaching a broad maximum value of ~+2.5‰ relative to V-SMOW (Swart, 2000) at 300 mbsf. At Site 1006, porewater $\delta^{18}O$ values show an initial increase from 0‰ to +0.7‰ at 75 mbsf, followed by a subsequent decrease to +0.2‰ downcore where it remains constant below 200 mbsf. This pulse at Site 1006 is consistent with the trapping of fluid from the last glacial maximum (Adkins and Schrag, 2003; Schrag et al., 2002). The significant downcore increase in fluid $\delta^{18}O$ values at Site 1003 (Fig. 4), also observed at Sites 1005, 1004, and 1007, can be attributed to a diffusive flux from below as it is accompanied by an increase in chlorinity (which reaches approximately double seawater concentrations at the bottom of the core), combined with recrystallization of carbonate sediments at elevated temperature (Swart, 2000, 2015).

As sediments recrystallize along the geothermal gradient in a diffusively limited system, the $\delta^{18}O$ values of pore fluids can become more positive, and carbonate sediments and

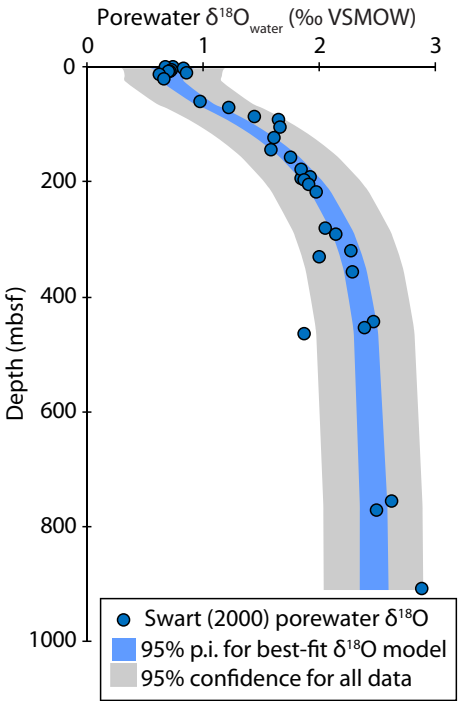

Fig. 4. Measured pore fluid $\delta^{18}O$ values (Swart, 2000) from Site 1003 and best-fit model for fluid composition. Flushed zone (upper 40 mbsf) $\delta^{18}O$ value is 0.7 ± 0.1‰; below which, values equilibrate to $+2.5 \pm 0.2$‰ over a scale distance of 135 ± 37 m.

corresponding fluids co-evolve with respect to one another. To this end, we have applied the clumped isotope paleothermometer to carbonate sediments in order to thermally constrain this system and estimate porewater $\delta^{18}O$ value.

1.2.3. Isotopic heterogeneity of Leg 166 sediments

Isotopic analyses (C and O) and X-ray diffraction (XRD) of sediments at these sites demonstrated a high degree of covariance between the mineralogy (e.g. abundance of aragonite) and $\delta^{13}C$ values, indicative of multiple sediment sources (Swart and Eberli, 2005). The $\delta^{18}O$ values from the same study (presented in this paper for the first time), however, reveal a diminished, but nonetheless significant co-variation with mineralogy where the LMC end-member had a more positive $\delta^{18}O$ value. This co-variation between $\delta^{18}O$ values and mineralogy suggests a relationship between either fluid $\delta^{18}O$ values or formation temperature and mineralogy. As a result of evaporation the $\delta^{18}O$ values of surfaces water on the GBB, the likely source of the aragonite end-member, are more positive than the surrounding marine waters (Swart et al., 2009). Therefore, if primary fluid $\delta^{18}O$ values were the governing factor in sediment composition, one would expect a more positive $\delta^{18}O$ value in aragonitic platform-derived sediments, precisely the opposite of the observed trend observed here. Therefore it is likely that some fraction of the LMC component formed at temperatures cooler than those at the sea surface. The $\delta^{18}O$ data and the interpretations regarding $\delta^{13}C$ values by Swart and Eberli (2005) can be consistent with one another if an additional calcite component is present that formed at a cooler benthic temperature in an environment where $\delta^{13}C$ values are also overprinted to some degree.

There is considerably more carbon in carbonate rocks than is present as dissolved inorganic carbon (DIC) in the corresponding fluids. A typical carbonate with ~65% porosity would require the flushing of approximately 9000 pore-volumes of water to replace all carbon. It is possible that a diagenetic end-member could have formed in an essentially open system either at the sediment-water interface or in a zone of significant advection such as the flushed zone described at these sites by Kramer et al. (2000). This flushed zone is typified by the uppermost (as deep as 50 mbsf) sediments' pore fluids retaining similar concentrations of conservative and non-conservative major and minor elements and O isotopic compositions as the benthic waters. Within this zone the pore fluid flow rate at ODP Sites 1005 and 1009 has been estimated to be 11 cm/year (Henderson et al., 1999). While the flushed zones at Sites 1003 and 1006 (20–40 mbsf) are not as pronounced as those closer to the platform (Sites 1005, 1004, and 1009) (~50 mbsf), it nevertheless is a distinctive feature at both Sites 1003 and 1006. Conversion of aragonite to calcite within this zone could occur with significant fluid exchange with benthic waters. It is also likely that some diagenetic end-members formed with contributions from respired organic carbon although below the flushed zone the system is rock buffered and such contributions are unlikely to be manifested in the sedimentary $\delta^{13}C$ values.

The interpretation that sediments are undergoing early diagenesis in an essentially open system is given credence by measurements of calcium isotopes by Higgins et al. (2018), who note that calcium isotopes exhibit similar open-system diagenetic behavior at ODP Site 1003. Because the diagenetic endmember may be difficult to differentiate from a pelagic end-member using only the mineralogy and $\delta^{13}C$ values presented by Swart and Eberli (2005), and because both the calcite and aragonite sediments consist predominantly of micritic mud, the polymorphic transition from aragonite to calcite is not associated necessarily with any significant change in sediment type.

In this study, we will investigate the behavior of temperature-sensitive $\delta^{18}O$ and Δ_{47} proxies in order to elucidate these processes. These proxies should be able to discriminate between the primary and diagenetic crystallization temperatures as Bahamian sediments initially in warm surface waters and are subsequently deposited at cooler benthic temperatures (Leaman et al., 1995; Lüdmann et al., 2016). Because the $\delta^{18}O$ value of fluid can change downcore, the $T\Delta_{47}$ values will provide unambiguous crystallization temperatures to constrain the co-evolution of carbonate and fluid oxygen isotopes. Analyses of calcite and dolomite limestones in the nearby Andros Core by Winkelstern and Lohmann (2016) show precisely this behavior, where sediments' $T\Delta_{47}$ values report warmer burial temperatures and more positive fluid $\delta^{18}O$ values. The diagenetic behavior of clumped isotopes in recrystallizing carbonate rocks in the Andros core and ODP Site 807, a low-latitude pelagic site, by Stolper et al. (2018). This study simulated the recrystallization of carbonate rocks at these sites where primary Δ_{47} values are overprinted by burial

temperatures. These simulations results were able to reproduce the observed trend in measured Δ_{47} values at the Andros core, showing the overprinting of primary temperatures with the warmer burial temperatures. Models for Site 807, a low-latitude pelagic site, indicated that the early diagenesis would preserve the cool benthic temperatures, and subsequent recrystallization would preserve the geothermal gradient. No comparable measurements have yet been published investigating burial diagenesis and porefluid $\delta^{18}O$ evolution using clumped isotopes for a modern carbonate platform margin, such a record would be useful as platform margin sediments constitute a significant fraction of the carbonate rock record. Analyses from periplatform carbonates recovered by ODP Leg 166 presented in this manuscript will be compared to the Andros core and a record of Phanerozoic dolomites in the discussion.

1.3. Application of clumped isotopes

The analyses of multiply-substituted isotopologues in natural materials, termed "clumped isotopes", provides a powerful tool for the study of diagenetic processes. Because the relative abundance of $^{13}C—^{18}O$ bonds in carbonate minerals compared to a stochastic distribution (Δ_{47}) is proportional to the temperature at which a mineral formed (Schauble et al., 2006), it can be used as an independent measurement of paleotemperatures (Eiler, 2011; Ghosh et al., 2006). This is especially useful in situations wherein the $\delta^{18}O$ value of the parent fluid of a mineral cannot be easily constrained or if secondary minerals form over a range of temperatures (Huntington et al., 2011; Mangenot et al., 2017; Staudigel et al., 2018).

The variation in downcore $\delta^{18}O$ values in porefluids, as well as the variable temperatures experienced by sediments, makes clumped isotopes an ideal proxy for studying the rate of sediment recrystallization. at these sites. Clumped isotopes, by virtue of behaving as a non-conservative property during carbonate recrystallization, are insensitive to rock-buffering effects. This makes it particularly suited to study the systems discussed herein, particularly the more deeply buried (and consequently more rock-buffered) sediments.

2. METHODS

2.1. Sample selection and preparation

Sediments were recovered by the shipboard scientific party on ODP Leg 166 using the SEDCO/BP 471 (JOIDES Resolution) (Eberli et al., 1997a). Samples were shipped to the University of Miami for analysis in heat-sealed plastic bags. Aliquots were taken from these bags, which were homogenized and stored in scintillation flasks or Eppendorf vials prior to analysis.

2.2. X-Ray Diffractometry (XRD)

The mineralogical data in this manuscript is derived from Swart and Eberli (2005), supplemented by additional analyses performed using identical methods as outlined by Swart et al. (2003). This technique uses cumulative areas of the aragonite 1,1,1 peak ($2\theta = 26.1°$), the calcite 1,0,1 peak ($2\theta = 29.4°$), the high-magnesium calcite 1,0,1 peak ($2\theta = 29.6°$) and the dolomite 1,0,4 peak ($2\theta = 30.8$) to calculate the relative abundance of each mineral.

Samples were ground into a slurry using an agate mortar and pestle and de-ionized water. This slurry was mounted onto 2.5 cm glass XRD slides and dried for at least >12 h. These slides were analyzed using a Panalytical X-Ray diffractometer, scanning between $2\theta = 25$ and 35° (Cu K-alpha emission, $\lambda = 1.54$ Å). Peak fitting was conducted using the X'Pert HighScore Plus software package, the relative areas of the relevant peaks were used to determine the relative abundance of the carbonate minerals (Swart et al., 2003).

2.3. Isotopic analysis

2.3.1. Stable C and O analyses

Samples were analyzed using a Finnigan-MAT251 mass spectrometer interfaced with a Fairbanks common acid bath device. The δ^{45} and δ^{46} data have been corrected for the usual isobaric interferences (Craig, 1957) modified for a triple collector mass spectrometer and calibrated to the Vienna Pee Dee Belemnite (V-PDB) scale using NBS-19.

2.3.2. Clumped isotope analyses

The methods for sample preparation for clumpedisotope analysis in this study are identical to those in previous publications from the University of Miami Stable Isotope Lab (Murray et al., 2016; Staudigel and Swart, 2016). Approximately 8–9 mg of carbonate sediment, placed in copper reaction boats and transferred to the carousel of a modified Fairbanks device attached to a common acid bath. Atmosphere is pumped out first with a rotary pump, then a greater vacuum ($<10^{-3}$ mbars) is maintained with a turbomolecular pump. Samples are reacted with concentrated phosphoric acid (1.93–1.95 g/cc, nominally 103–105% H_3PO_4), liberated CO_2 and H_2O gas are continually captured in trap cooled with liquid nitrogen. The CO_2 and H_2O are separated from one another by thawing the trap with a −90 °C methanol slush, which allows for CO_2 to sublimate while H_2O remains frozen. The CO_2 gas is captured in another trap and is subsequently passed through a Porapak™ column chilled to between −20 to −30 °C. The resulting clean, dry gas is transferred to a Thermo-253 mass spectrometer for analysis.

Sample gas is analyzed using a dual-inlet method which alternates between analysis of sample gas and an in-house reference "working gas". Beam intensities of $M/Z = 44$–49 are measured in blocks of analyses. Each block consists of 4 "off peak" measurements and 16 "on peak" followed by 4 "off peak" measurements. The off peak analyses measure the negative pressure baseline at mass 47, which is added to the on peak measurements (He et al., 2012).

Isotope ratios for the sample gas are calculated relative to the in-house working gas, which is calibrated relative to the NBS-19 standard. Carbon and oxygen isotope ratios are reported in the conventional notation relative to the V-PDB standard. Subsequent calculations for absolute iso-

tope abundance use the "Brand Parameters" recommended by Daëron et al. (2016). Oxygen isotopes for carbonates are calculated using the gas $\delta^{18}O$ values by correcting for acid fractionation at 90 °C using the fractionation factor calculated by Swart et al. (1991).

The abundance of mass-47 CO_2, compared to that expected in a stochastically distributed gas is expressed as Δ_{47}, which is calculated using the methods defined by Huntington et al. (2009). The equilibrated standards used in the Miami Stable Isotope Laboratory are CO_2 gas equilibrated with water at 25 °C and 50 °C, as well as CO_2 equilibrated in quartz tubes at 1000 °C, which are used to establish an empirical transfer function for "raw" Δ_{47}, converting them to an absolute reference frame (Dennis et al., 2011). An acid fractionation factor of 0.092‰ is added to aragonite, calcite and HMC (Passey et al., 2010), and 0.152‰ is used for dolomite (Murray et al., 2016). No sample consisted purely of dolomite, the highest abundance in any sample measured for clumped isotopes was 15% dolomite. For these mixed mineralogy samples, a weighted acid fractionation factor is applied using the fractional mineralogy calculated using XRD, this amounted to a maximum difference in final Δ_{47} value of <0.01‰.

Temperatures are calculated using the temperature-Δ_{47} relationship published by Staudigel et al. (2018), which was produced using identical acid digestion, preparation and analytical techniques and has been calibrated to material precipitated at known temperatures between 5 °C and 73 °C.

$$\Delta_{47} = \frac{0.0400(\pm 0.0013) \times 10^6}{T^2} + 0.245 \quad (\pm 0.014) \tag{2}$$

In figures, error bars correspond to the standard error of all analyses conducted on a sample, reported temperatures are the temperature from these mean values, and the reported uncertainty is the difference between the temperature of the mean and the mean + standard error. This technique, as opposed to calculating temperatures for each individual analysis, ensures that the mean temperature is always calculated from the mean Δ_{47} value, this same method is also applied to calculating $\delta^{18}O$ values of fluids. These two techniques for calculating error in $T\Delta_{47}$ and reconstructed fluid $\delta^{18}O$ values yield very similar results, however.

2.3.3. Calculation of fluid $\delta^{18}O$ values using clumped isotope measurements

Using carbonate $\delta^{18}O$ and $T\Delta_{47}$ values, the $\delta^{18}O$ value of the water from which carbonate minerals formed can be estimated using published alpha-temperature relationships. Because different carbonate minerals fractionate oxygen isotopes differently, a unique $\alpha_{water\text{-}carbonate}$-temperature relationship is calculated for each sample using the following equation.

$$\alpha^{sample}_{water-calcite} = F_{aragonite}\alpha^{aragonite}_{water-calcite} + F_{calcite}\alpha^{calcite}_{water-calcite} + F_{dolomite}\alpha^{dolomite}_{water-calcite} \tag{3}$$

For this study, the alpha-temperature relationships used for calcite (Kim and O'Neil, 1997), aragonite (Kim et al., 2007) and dolomite (Matthews and Katz, 1977) are shown in Table 1. Using percentage of the different carbonate minerals, it is possible to reconstruct the $\delta^{18}O$ value of fluids from which the mineral formed. The $\delta^{18}O$ value of the carbonate measured using the 253 is used to calculate the fluid $\delta^{18}O$ value. These values are reported relative to the conventional Vienna Standard Mean Ocean Water (V-SMOW) reference frame. There is a small discrepancy when applying this to mixed systems of primary and secondary minerals, this is due to the non-linearity of $\alpha_{water\text{-}calcite}$ and Δ_{47} – temperature relationships. A 50% mixture of aragonite formed at 30 °C from a parent fluid whose $\delta^{18}O$ value is 0‰ and calcite formed at 10 °C from the same fluid predicts a $T\Delta_{47}$ value of 19.5 °C and a parent fluid $\delta^{18}O$ value of −0.04‰. Similar deviations from a simple mixing line are found when different fluid compositions are used in the same model, however these differences never exceed the standard deviation of replicate analyses. However, this effect consistently biases mixtures of materials of the compositions expected in Leg 166 sediments towards slightly cooler (−0.5 °C) and slightly more negative (−0.04‰) $\delta^{18}O_{fluid}$ values.

In some diagenetic regimes, kinetic isotope effects present an obstacle for the accurate reconstruction of paleotemperatures using $\delta^{18}O$ and Δ_{47} thermometry (Defliese and Lohmann, 2016; Loyd et al., 2016). For example, in situations where microbially produced CO_2 contributes to the dissolved carbonate, the oxygen bound to the respired carbonate may be disequilibrated with respect to present fluid composition and temperatures (Thaler et al., 2017). To date, no studies have directly demonstrated that clumped isotopes in respired carbon are similarly disequilibrated, although measurements of modern and ancient methane seeps provide some circumstantial evidence for this (Loyd et al., 2016). As DIC approaches equilibrium, intermediate Δ_{47} values may be apparently disequilibrated even if the initial and equilibrium Δ_{47} values are identical; this is due to a kinetic difference in ^{12}C and ^{13}C oxygen isotope equilibration rates (Staudigel and Swart, 2018). In zones where rates of carbonate precipitation are so rapid that $\delta^{18}O$ and Δ_{47} values of the DIC have insufficient time to equilibrate prior to mineralization, these disequilibrated states may be preserved. This effect has been demonstrated in a laboratory setting by Guo et al. (2019), who facilitated

Table 1
Published relationships between oxygen isotope fractionation and temperature for Calcite, Aragonite and Dolomite.

Mineral	$1000\ \ln\alpha_{carbonate\text{-}water}$	Source
Calcite	$18.03 \times 10^3\ T^{-1} - 32.42$	Kim and O'Neil (1997)
Aragonite	$17.88 \times 10^3\ T^{-1} - 31.14$	Kim et al. (2007)
Dolomite	$3.06 \times 10^6\ T^{-2} + 0.11$	Matthews and Katz (1977)

the aragonite-to-calcite neomorphic transition and demonstrated that the conversion at 90 °C was sufficiently rapid that the isotopic configuration of DIC had insufficient time to equilibrate. In addition, rapid rates of mineral formation particularly in alkaline environments, are expected to exhibit kinetic isotope disequilibrium effects due to incomplete reverse reactions at the mineral-fluid boundary layer (Watkins and Hunt, 2015; Watkins et al., 2014). The reaction rates associated with the dissolution of aragonite and precipitation of calcite discussed in this manuscript appear to occur over thousands of years, and are thus likely to reflect a near-equilibrium process with respect to the equilibration of DIC. Analyses of slow-growing calcite in Devil's Hole by Kluge et al. (2014) yielded Δ_{47} values within the uncertainty of synthetic calcites (Zaarur et al., 2013), albeit slightly more positive. The $\delta^{18}O$ analyses of the same material were disequilibrated by over 1‰, however. It is possible that the kinetic effects on the $\delta^{18}O$ and Δ_{47} values may result in some deviation from the authors' choice of calibrations for oxygen isotopes (Kim and O'Neil, 1997; Kim et al., 2007; Matthews and Katz, 1977) and clumped isotopes (Staudigel et al., 2018); the authors acknowledge that application of synthetic calibrations to natural systems may impart some error to their interpretations.

2.4. Time-integrated modeling

In order to simulate the effect of different sediment accumulation histories for Sites 1003 and 1006 on similarly reactive materials, time-integrated models have been constructed for both sites. Different simulations are run using the sediment accumulation histories of both sites with different reactive behaviors. These models output a prediction the carbonate $\delta^{18}O$ and Δ_{47} values given these assumptions. The preservation of initial isotopic composition as well as its overprinting by diagenetic temperatures and fluid compositions are tested, along with the preservation of different fluid isotopic compositions. As these models are intended to be illustrative of the different ways sediment accumulation rate and recrystallization rate affect the final composition, and not to be used as absolute statements of fact, no attempt was made to "fine tune" these models.

Several potential diagenetic simulations were tested for Sites 1003 and 1006, in which different recrystallization rates were simulated. In the case of Site 1003, two different downcore fluid $\delta^{18}O$ histories were modelled. Over each model, the depositional history was divided into 500 time steps of 46 or 26 kyr for Sites 1003 and 1006 respectively. This approach is derived from the model used by Schrag et al. (1995), modified such that the model assumes an initial composition of sediments and simulates the $\delta^{18}O$ and Δ_{47} values for each sedimentary unit over time. The sedimentation rate over each time step was calculated using the age-depth model used by Swart and Eberli (2005), adjusted for compaction. In the model, after each new sediment package is deposited underlying sediments are compacted and temperatures and fluid $\delta^{18}O$ values calculated. Sediments undergo recrystallization where a fraction of carbonate is recrystallized at equilibrium with current burial conditions. This model is derived from the model used by Staudigel et al. (2018), modified such that sediments are initially pure carbonate which subsequently recrystallizes. This approach is similar to the model constructed by Stolper et al. (2018) to describe a number of pelagic and shallow carbonate sites.

Compaction of sediments was estimated using the downcore porosity for Site 1003 (Fig. 5a) and Site 1006 (Fig. 5b) (Berner, 1980). This approach assumes that the extent of compaction of any unit of sediment is proportional to the mass of overlying sedimentary units, resulting in porosity (φ) following a first-order exponential relationship with depth.

$$\varphi(depth) = \varphi_{eq} - (\varphi_{eq} - \varphi_i)e^{-depth/D_{scale}} \quad (4)$$

In this equation, φ_i is the porosity of unburied sediment, and φ_{eq} is the porosity at infinite burial depth. The rate of compaction downcore is defined by the scale depth, D_{scale}. It is apparent in Fig. 5 that there is considerable deviation from this first-order downcore relationship between porosity and depth at both sites, the regression coefficients for Sites 1003 and 1006 were 0.56 and 0.46 respectively. This is evidenced by the broad confidence interval (gray regions) for both regressions with more variance at Site 1003. Despite this, these parameters will be used to simulate compaction in models as they best describe the compaction history of core as a whole; or at least provide a reasonable approximation of it.

The modern porewater gradient in $\delta^{18}O$ values was approximated using a first-order equilibration model, which is forced to remain constant over the uppermost 40 mbsf in order to simulate the flushed zone. Below 40 mbsf, the fluid $\delta^{18}O$ values are fitted using Eq. (5).

$$\delta^{18}O_p(depth) = \delta^{18}O_{eq} - (\delta^{18}O_{eq} - \delta^{18}O_{flush})e^{-depth/D_{scale}} \quad (5)$$

As shown in Fig. 4 for Site 1003 where the value for the flushed zone is 0.74 ± 0.06‰, the equilibrium $\delta^{18}O$ value is 2.5 ± 0.2‰, the scale depth (D_{scale}) for oxygen isotopes is 135 ± 37 m (±95% confidence for all parameters). Site 1006 was modeled using a vertical fluid $\delta^{18}O$ gradient which increases by 1‰ from the latest Miocene to the present day to account for changes in ice volume.

A second iteration of each model was run for Site 1003 such that the equilibrium $\delta^{18}O$ value was initially double its present value (+5‰) and decreased between 10 Ma and present to its present-day value. This was aimed at investigatin the potential for preservation of a previously enhanced $\delta^{18}O$ gradient.

Three families of recrystallization rates were tested, to investigate three possible diagenetic regimes: an initial pulse of recrystallization, a constant rate of recrystallization and a pulse which decreases to a slower constant rate. Additional models were run for each of these rates where diagenetically altered material continued to recrystallize at some fraction (β) of the initial rate of recrystallization. The rate of recrystallization was calculated using an exponential decay function, following the form proposed by Richter and DePaolo (1987), where the rate (R) decreases over time

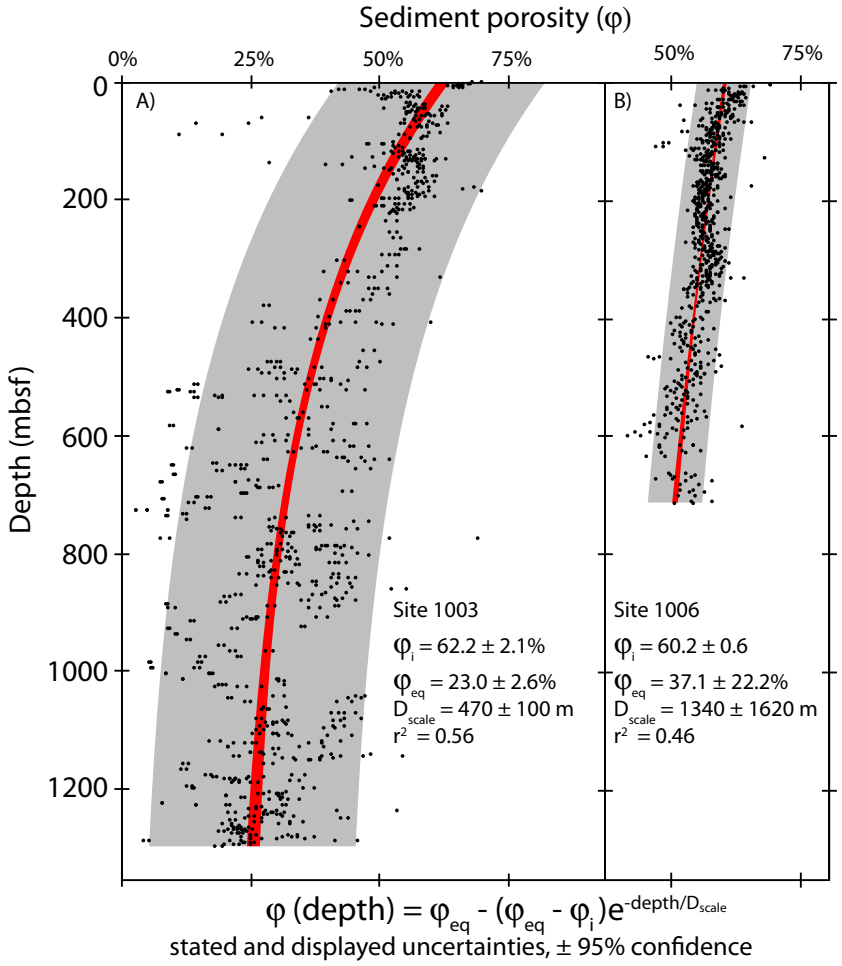

Fig. 5. Measured porosity with best-fit downcore exponential equation. Gray region 95% confidence interval, red region: ±95% confidence. (A) Site 1003, (B) Site 1006. Data from Eberli et al. (1997b).

after sediments are emplaced. This is defined using the following notation.

$$R = A + Be^{-age/C} \quad (6)$$

Each of these models was run three times with authigenic carbonate being modeled as being either as reactive as the primary material ($\beta = 1$), or less reactive (β 0.5 or 0.1). The rate of recrystallization (primary + secondary) for each of these models over time is shown in Fig. 6. In total, 27 simulations were run which generated $\delta^{18}O$ and Δ_{47} values downcore for a variety of recrystallization and porewater $\delta^{18}O$ behaviors. Eighteen of these simulations used the sediment accumulation history for Site 1003 and nine used the sediment accumulation history for Site 1006. Three sets of recrystallization rate parameters were used in the models, which simulate either an initial pulse of recrystallization which decays over time to zero, continuous recrystallization, or an initial pulse of recrystallization followed by a slower constant rate. The models which used the sediment accumulation history for Site 1003 were simulated using two different gradients of porewater $\delta^{18}O$ values over time in order to test the preservation of potentially different downcore porefluid gradients in the past. The first model used the modern porewater $\delta^{18}O$ downcore gradient (Fig. 4) throughout the entire depositional history. The second set of simulations used a more positive gradient which equilibrates to 5‰ at depth until 10 Ma, after which the equilibrium $\delta^{18}O$ value decreases into the modern. This second model is aimed to test which recrystallization behavior would record enhanced porewater $\delta^{18}O$ gradients during the past.

3. RESULTS

3.1. Site 1006 Composition

The mineralogy, $\delta^{13}C$, $\delta^{18}O$ $T\Delta_{47}$, and reconstructed water $\delta^{18}O$ values for Site 1006 are provided in supplementary tables and are displayed in Fig. 7. A 19-point mean was run through all measured $\delta^{13}C$ and $\delta^{18}O$ values and is shown as a shaded region in Fig. 7 defining ±95% confidence of mean. A 9-point mean is shown for clumped isotope measurements and reconstructed fluid $\delta^{18}O$ values.

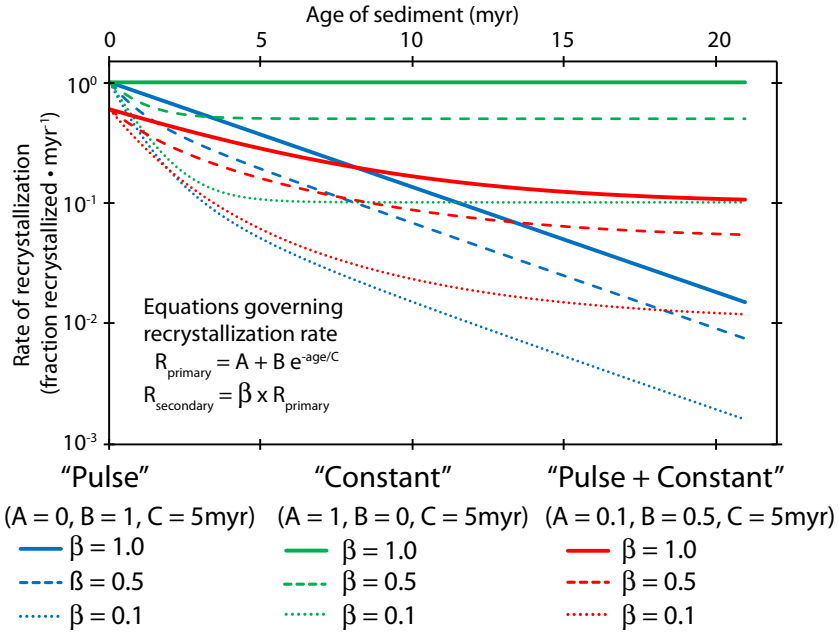

Fig. 6. Reaction rates compared to sediment age used for different model runs.

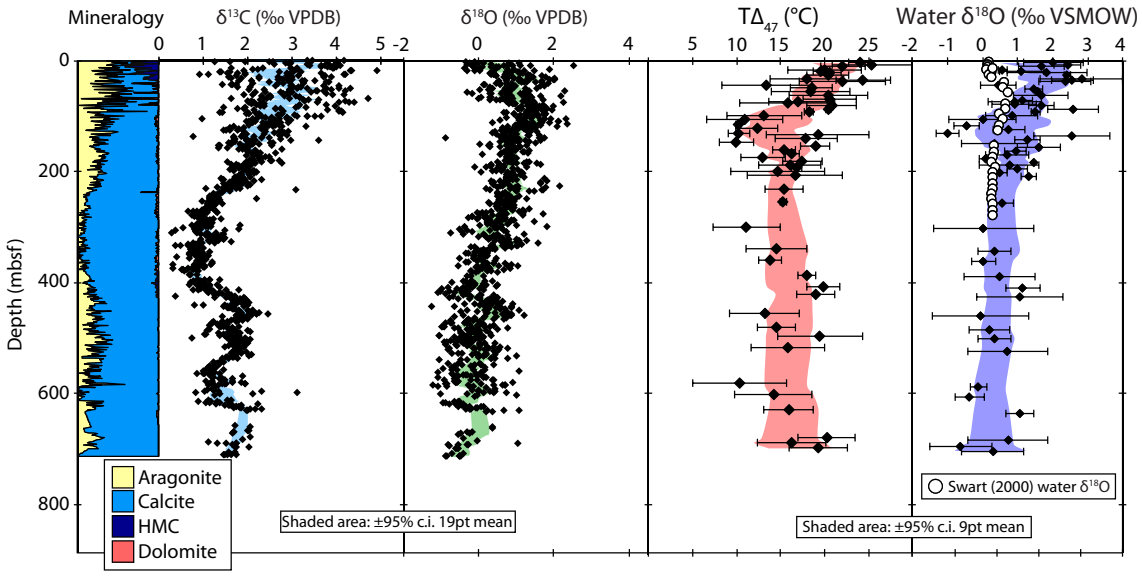

Fig. 7. Mineralogy, $\delta^{13}C$, $\delta^{18}O$ $T\Delta_{47}$ and water $\delta^{18}O$ values reconstructed using clumped isotopes for ODP Site 1006 plotted relative to depth. Mineralogy and carbon isotopic data from Swart and Eberli (2005).

Aragonite and calcite comprise the majority of sediments' mineralogy at Site 1006, along with traces of HMC in the uppermost 100 mbsf and traces of dolomite below 200 mbsf. The uppermost sediments at Site 1006 consists of a highly variable mixture of aragonite and calcite which reaches a point of maximum abundance of calcite at approximately 300 mbsf. Below this point, aragonite is once again present, although the mineral typically comprises less than 30% of the sediment.

The $\delta^{13}C$ values range between +5‰ and +0.5‰ at Site 1006. The uppermost sediments show substantial spatial variability, varying as much as 4‰ between samples only meters apart. This variance decreases downcore, as sediments converge to a minimum $\delta^{13}C$ value of 1‰. Carbonate $\delta^{13}C$ values vary towards the bottom of the core, with the majority of variance in $\delta^{13}C$ coinciding with increases and decreases in the abundance of aragonite.

Carbonate $\delta^{18}O$ values at Site 1006 ranged between −0.5 and +2‰ relative to VPDB. Over the upper ~100 mbsf, $\delta^{18}O$ values increased from 0‰ at the sediment-water interface to +1‰ at 100 mbsf. Below this depth, the $\delta^{18}O$ values decrease to the bottom of the core, where values range between −0 and +1‰, showing more variance than at the top of the core.

Temperatures calculated using the clumped isotope proxy ranged between 25 °C and 8 °C. The composition of the uppermost sediments are characterized by a trend in reconstructed temperatures from 25 °C at the sediment-water interface to a minimum value of 15 °C below 200 mbsf. Reconstructed temperatures do not vary significantly downcore below this depth.

Water $\delta^{18}O$ values reconstructed using clumped isotopes range between −1 and +3‰. Reconstructed fluid $\delta^{18}O$ values become more negative in the uppermost sediments, transitioning from +2‰ at the sediment-water interface to a broad minimum value of 0‰.

3.2. Site 1003

The mineralogy, $\delta^{13}C$, $\delta^{18}O$, $T\Delta_{47}$, and reconstructed water $\delta^{18}O$ values for Site 1003 are provided as a dataset and are displayed in Fig. 8. A 19-point mean was run through all measured $\delta^{13}C$ and $\delta^{18}O$ values and is shown as a shaded region in Fig. 8 defining ±95% confidence of mean. A 9-point mean is shown for clumped isotope measurements and reconstructed fluid $\delta^{18}O$ values.

Sediments consisted predominantly of aragonite and calcite, as well as trace HMC in the uppermost sediments and trace dolomite in deeper sediments. The uppermost 150 mbsf are predominantly aragonite followed by a steep decline in aragonite abundance, with LMC eventually compromising >90% of the total carbonate material.

The $\delta^{13}C$ values at Site 1003 range between +5 and +1‰. The $\delta^{13}C$ values of the uppermost sediments were the most positive, trending towards more negative values with depth. Below 200 mbsf, there was no significant trend until ~1000 mbsf, where sediment $\delta^{13}C$ values become slightly more negative downcore.

Carbonate $\delta^{18}O$ values at Site 1003 ranged between −1 and +3‰. Over the upper 200 mbsf, $\delta^{18}O$ values increased from 0‰ at the sediment–water interface to +2.5. Below 200 mbsf, $\delta^{18}O$ values vary between +1.5 and +2.5. Below 600 mbsf, $\delta^{18}O$ values decrease to the bottom of the core, where values range between −1 and +1‰, with more variance than observed at the top of the core.

Temperatures calculated using clumped isotopes ranged between 45 °C and 8 °C. Overall, the uppermost 200 mbsf displays a trend from 25 °C at the sediment-water interface to a minimum value, averaging 13 °C. Below this depth, sediments record warmer temperatures downcore, reaching a broad maximum temperature around 35 °C in most deeply buried sediments.

Fluids reconstructed using clumped isotopes range between −1 and +7‰ relative to VMSOW and show no significant change in the uppermost sediments, averaging +1‰. Below 250 mbsf, reconstructed fluid $\delta^{18}O$ values

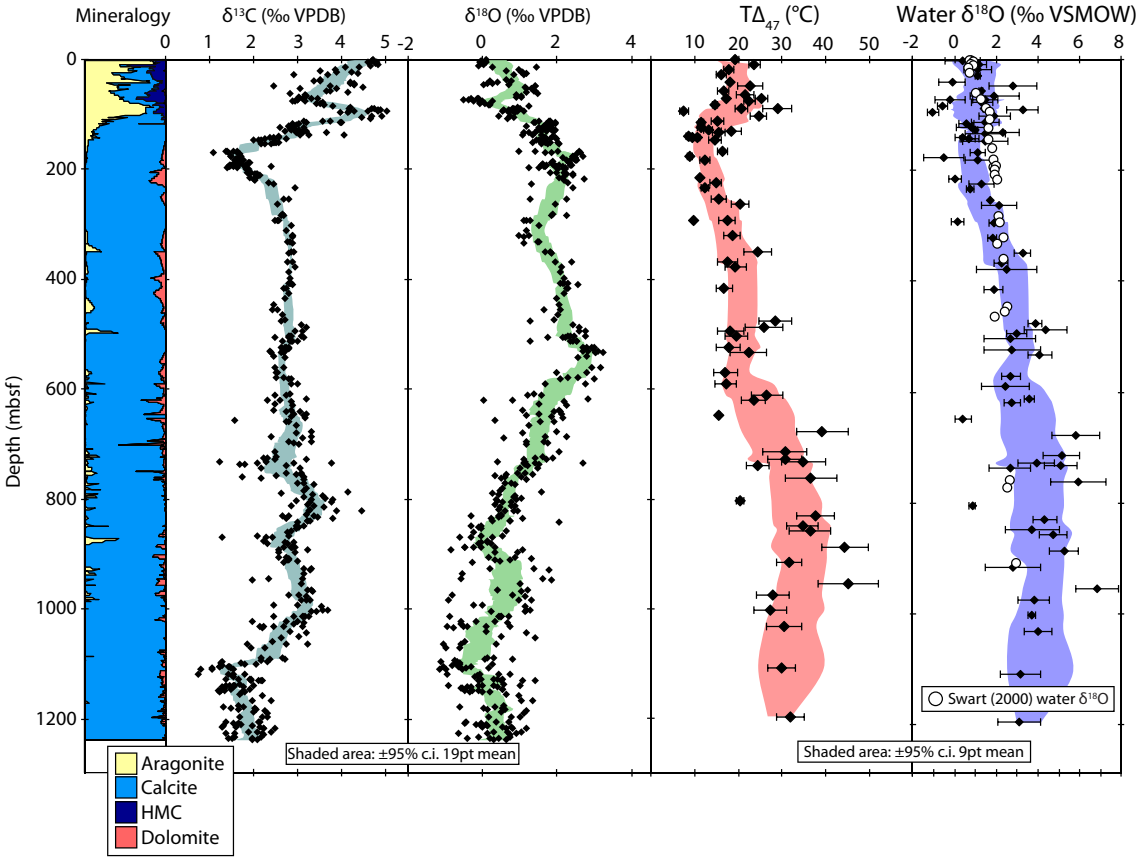

Fig. 8. Mineralogy, $\delta^{13}C$, $\delta^{18}O$, $T\Delta_{47}$ and water $\delta^{18}O$ values reconstructed using clumped isotopes for ODP Site 1003 plotted relative to depth. Mineralogy and carbon isotopic data from Swart and Eberli (2005).

become more positive, reaching a maximum value of +4‰ below 600 mbsf.

3.3. Time-integrated model results

The modeled $T\Delta_{47}$ and reconstructed fluid $\delta^{18}O$ values for Site 1003 are displayed in Fig. 9, and are compared to the 95% confidence interval of the 9-point mean for the measured values at Site 1003. Model results for Site 1006 are displayed in Fig. 10, and are compared relative to the 95% confidence intervals for measured $\delta^{18}O$ and $T\Delta_{47}$ values shown in Fig. 7. Because models with different $\delta^{18}O$ values for pore fluids still reproduce identical $T\Delta_{47}$ trends, Fig. 9a shows the downcore trends for both fluid models. Fig. 9b shows the reconstructed fluid $\delta^{18}O$ values for models using only the modern gradient in porewater $\delta^{18}O$ values, and Fig. 9c shows the results for models where the porewater $\delta^{18}O$ gradient peaked at 5‰ at depth.

The models for Sites 1003 and 1006 show similar behavior for $T\Delta_{47}$ to one another, although differences can be observed between Figs. 9a and 10a, which are attributable to differences in accumulation history. The $T\Delta_{47}$ values in the uppermost sediments for all models trended towards cooler temperatures, below a depth of 200 mbsf the models diverged from one another. The constant recrystallization model (Green lines: A = 1, B = 0) had the steepest gradient below 200 mbsf, however, this is only the case if diagenetic material is allowed to continue recrystallizing at the same rate as primary material (β = 1, solid line), models where diagenetic material is treated as "stabilized" (β = 0.5 dashed line, or 0.1 dotted line) did not record warmer burial temperatures. The "pulse + constant" (Red lines: A = 0.1, B = 0.5, C 5 myr) showed a similar behavior, although it was invariably cooler than the constant models (green line). The pulse model recorded the coolest temperatures when diagenetic material was modeled as less reactive (β = 0.1, dotted line), when diagenetic material was treated as being as reactive as the primary material (β = 1.0, solid line), the model trended towards warmer temperatures, although it began to flatten out at depth.

Models in which the gradient in the $\delta^{18}O$ values of porewater remained identical to the modern over time tended to converge at the deeper equilibrium value of 2.5‰ at depth as shown in Fig. 9b, varying only in the rate at which they approached equilibrium. Models where recrystallized material was more stable were more sensitive to initial conditions and thus the depositional hiatuses at 900 mbsf and 1100 mbsf were associated with negative excursions, which resembled the pore fluid $\delta^{18}O$ gradient. Below 400 mbsf, the absolute value of the reconstructed fluid $\delta^{18}O$ values for

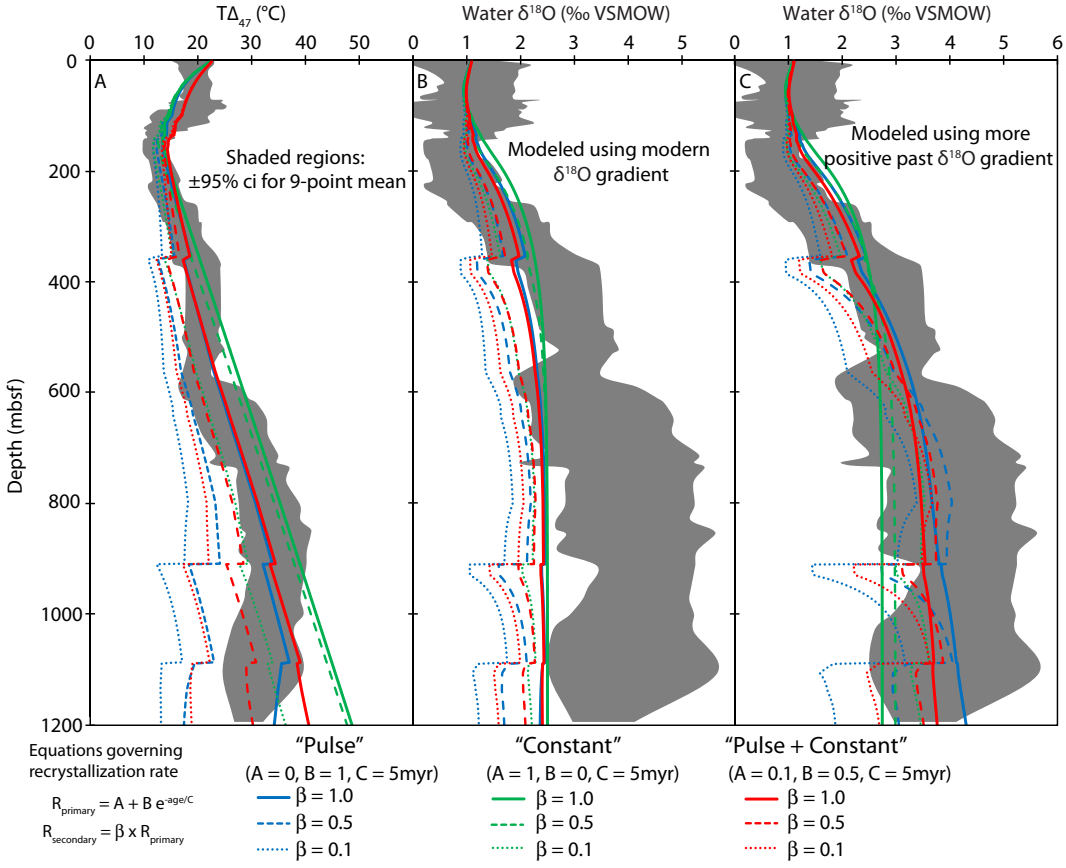

Fig. 9. (A) Measured and modeled $T\Delta_{47}$ values for Site 1003, (B) Measured and modeled $\delta^{18}O$ values reconstructed using clumped isotopes, models use constant downcore fluid $\delta^{18}O$ gradient. (C) Measured and modeled $\delta^{18}O$ values reconstructed using clumped isotopes, models use variable downcore fluid $\delta^{18}O$ gradient, with more positive downcore $\delta^{18}O$ values in Miocene.

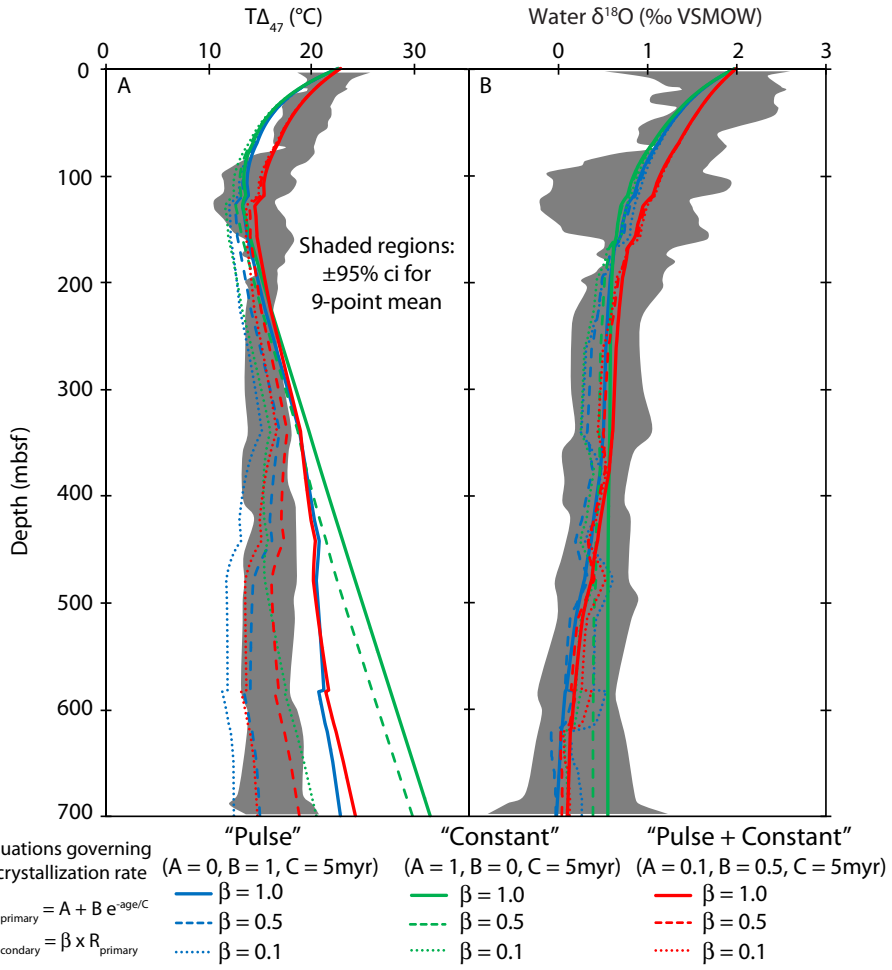

Fig. 10. (A) Measured and modeled $T\Delta_{47}$ values for Site 1006 and (B) Measured and modeled $\delta^{18}O$ values reconstructed using clumped isotopes.

these models is consistently lower than that which was measured at this site. Because no downcore variations were simulated for Site 1006, and fluid $\delta^{18}O$ emulated contemporary seawater values, models for Site 1006 recreated the observed trend towards more negative $\delta^{18}O$ values, which corresponds to the evolution of marine $\delta^{18}O$ values since the Neogene.

In models where the Miocene pore fluid $\delta^{18}O$ gradient was double its present value, the reconstructed fluid $\delta^{18}O$ from clumped isotopes is more positive (Fig. 9c). Models where sediments become less reactive over time preserve the most positive values (Blue lines), models where sediments become less reactive, but nevertheless continue to react at a constant rate at depth (red lines) likewise record these more positive fluid $\delta^{18}O$ values. The continually recrystallizing models (green lines) are nearly identical between the two pore water models, as a consequence of the model having sufficient time for sediments to overprint their initially more positive $\delta^{18}O$ value. In these models, if the diagenetic fraction is less reactive than unaltered sediment ($\beta = 0.1$ or 0.5), reconstructed fluids from clumped isotopes are more positive (dotted and dashed green lines in Fig. 9c).

Models using Site 1003's sediment accumulation history simulating sediments which become stabilized ($\beta = 0.1$ or 0.5) preserve rapid negative excursions in $\delta^{18}O$ and $T\Delta_{47}$ in sediments at 350, 900 and 1100 mbsf. These excursions are related to depositional hiatuses at these depths, and models which bias the final composition towards earlier diagenetic conditions tend to preserve these events more strongly. Sediments which continue to react during later burial do not preserve geochemical evidence for these early events as strongly.

4. DISCUSSION

4.1. Uppermost sediments: end-member sediment mixing and early diagenesis

The sediments deposited along the margins of GBB consist of platform-derived sediments and pelagic sediments. These two end-members are isotopically and mineralogi-

cally distinct from one another. End-member mixing of these sediments occurs in the uppermost strata, where a strong degree of covariation has been observed at all sites on the Leg 166 transect between the mineralogy (e.g. the abundance of aragonite) and $\delta^{13}C$ values of the sediments (Swart and Eberli, 2005). This variance is correlated with changes in sedimentary motif in the core description. This can be observed in the large slump deposits described by Betzler et al. (1999) between 80 and 110 mbsf at Site 1003 (Fig. 11). These slump deposits are accompanied by an increased abundance of aragonite, along with corresponding changes in $\delta^{13}C$ and $\delta^{18}O$ values. The diminishing abundance of peloidal material downcore at Site 1003 correlates with the observed changes in isotopic composition downcore, where the appearance of peloids in sediments above ~150 mbsf marks the onset of a trend towards warmer temperatures reconstructed using oxygen and clumped isotopes, as well as more positive $\delta^{13}C$ values (Fig. 11).

Site 1006 consists predominantly of channel drift deposits (Fig. 2), which are transported by the strong currents in the channel, and exhibit no significant changes in sedimentary motif throughout the uppermost sediments, consisting predominantly of a mud-wackestone (Betzler et al., 1999) (Fig. 12). Although there are no significant changes in sediment lithology, these sediments are extremely heterogeneous in mineralogy and isotopic composition (Fig. 12). The abundance of pelagic and platform-derived sediments at Site 1006 is interpreted to reflect changes in sediment source over glacial-interglacial cycles (Swart and Eberli, 2005). There is an apparent broad trend towards a LMC endmember over the uppermost sediments of Site 1006 (Fig. 12). Over this interval sediment Δ_{47} values reconstruct cooler temperature, suggesting that the broader trend is a result of neomorphism of aragonite to calcite, as well as recrystallization of primary calcite allochems.

At Site 1003, this covariance between aragonite abundance and $\delta^{18}O$ ($r^2 = 0.66$, $n = 156$) and $T\Delta_{47}$ ($r^2 = 0.37$, $n = 31$) values has been observed in sediments from the uppermost 200 mbsf sediments (Fig. 13). The covariance between temperature-sensitive proxies and mineralogy in the uppermost sediments at Site 1003 suggest that the LMC endmember formed at considerably cooler temperatures than the aragonite endmember. Linear regression through all samples in the uppermost 200 mbsf indicate that the LMC endmember formed at 11.8 ± 3.2 °C (95% confidence), whereas the aragonite endmember formed at 23.0 ± 3.7 °C (95% confidence) (Fig. 13). The LMC endmember, therefore, formed at a considerably cooler temperature than modern surface temperatures. This is consistent with neomorphism occurring on the seafloor at the cooler, benthic temperature. While these temperatures are slightly cooler than expected surface and benthic temperatures, the difference between the two values is consistent with the vertical temperature gradient in the present day water column (Leaman et al., 1995; Lüdmann et al., 2016).

The covariance between the $\delta^{13}C$ values and mineralogy is generally consistent with sediment mixing, however, early diagenesis may also partially affect isotopic compositions in this manner. In a hypothetical pure carbonate sediment package with a DIC abundance of 3 mM and a porosity of 65%, it would require exchange with over 9,000 equivalent pore volumes in order to replace the carbon in the sediment. A flushed zone was observed in the porewaters of these sediments by Kramer et al. (2000) and (Swart, 2000) and it may provide such a mechanism, as pore waters as deep as 40 mbsf were chemically indistinguishable from benthic waters suggesting considerable advection of fluids. Calcium isotopes, which are similarly rock buffered in carbonate sediments (Fantle and DePaolo, 2007), show a corresponding change towards open-system behavior at Site

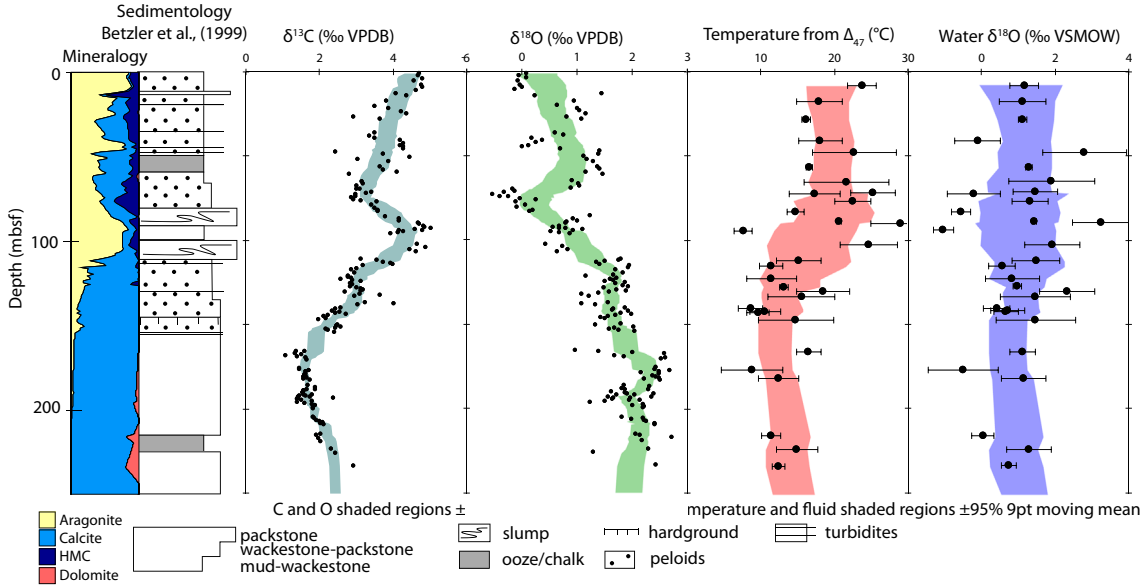

Fig. 11. Mineralogy, sedimentology, and $\delta^{13}C$, $\delta^{18}O$ and Δ_{47} values for upper 250 mbsf of Site 1003. Mineralogy and carbon isotopic data from Swart and Eberli (2005).

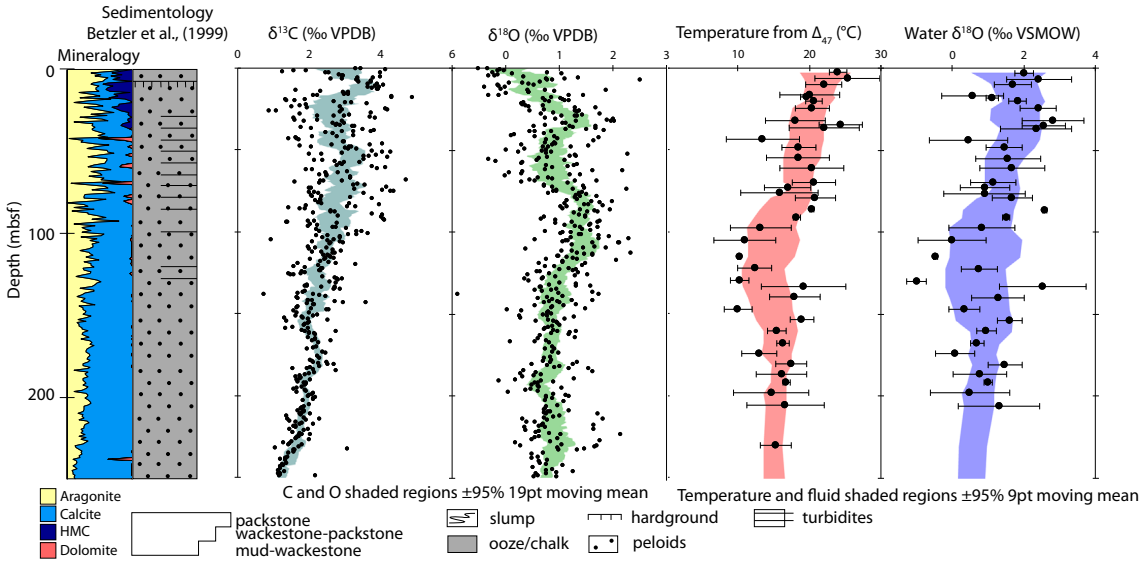

Fig. 12. Mineralogy, sedimentology, and $\delta^{13}C$, $\delta^{18}O$ and Δ_{47} values for uppermost 250 mbsf of Site 1006. Mineralogy and carbon isotopic data from Swart and Eberli (2005).

1003 (Higgins et al., 2018). Calcium isotopes are useful in this instance because primary sediments tend to be fractionated relative to the $\delta^{44/40}Ca$ values of the formation waters as a result of rate-dependent fractionation factor (Gussone et al., 2005; Lemarchand et al., 2004), slower diagenetic processes do not have this fractionation (Fantle and DePaolo, 2007) and thus authigenic carbonate tends to reflect the fluid from which it formed. Models of calcium and magnesium isotopes at Site 1003 by Ahm et al. (2018) demonstrate the enhanced degree of open system recrystallization in the uppermost sediments. The $\delta^{13}C$ values do not show a significant relationship with changes in global marine values as reported by Zachos et al. (2001) benthic foraminiferal $\delta^{13}C$ record (Fig. 15a). These values instead are affected by a mixture of local sediment mixing and diagenetic processes (Swart and Eberli, 2005). A period of minimal sediment accumulation at both Sites 1003 and 1006 between 2 and 3 Ma corresponds to the most negative $\delta^{13}C$ values at Site 1006, and Site 1003 is slightly more negative immediately below this (Fig. 15), this is likewise true for $\delta^{44/40}Ca$ values at Site 1003 (Higgins et al., 2018). Clumped isotopes, which are insensitive to fluid or rock buffering provide a unique insight into this system. Coherence between the minima in $T\Delta_{47}$ and $\delta^{13}C$ values, as well as the maxima in $\delta^{18}O$ and $\delta^{44/40}Ca$ values at a depth of ~200 mbsf illustrates agreement between the rate of recrystallization estimated using these mechanisms as well as indicating that this process occurred within a fluid-dominated open system.

The uppermost sediments at Site 1006 behave like a conventional end-member mixing model of sediments that originated in warm water. There is a high degree of covariance between mineralogy and $\delta^{13}C$ ($r^2 = 0.59$, $n = 291$), however, the temperature-sensitive $\delta^{18}O$ ($r^2 = 0.18$, $n = 291$) and Δ_{47} ($r^2 = 0.02$, $n = 36$) isotope proxies did not covary as significantly with mineralogy. Whereas the sediments do show a downcore trend towards cooler values, the extreme sediment heterogeneity appears to be driven by mixing of sediment sources rather than a larger diagenetic trend. Linear regression through the mineralogy and isotopic composition of the upper 200 mbsf sediments at Site 1006 indicates that the LMC endmember formed at 16.3 ± 3.3 °C (95% confidence) and the aragonite end member formed at 19.9 ± 5.6 °C (95% confidence), with no significant correlation between mineralogy and temperature ($p = 0.39$, $n = 36$).

At 4 Ma, the Δ_{47} values at both sites indicate an average temperature of around 13 °C (Fig. 15c). If this low temperature is a result of the overprinting of the initial surface temperature of ~25 °C at a benthic temperature of 10 °C, this would indicate that sediments have recrystallized approximately 80% at the benthic temperature. It is possible that benthic temperatures in the channel were depressed during periods of glaciation, which would necessitate less recrystallization to create the same effect. These back-of-the-envelope calculations for recrystallization rate (20%/myr) exceed the estimated rate from pore fluid Sr gradients (2–5%/myr), however, advection in the uppermost sediments in the flushed zone (Kramer et al., 2000) and authigenic celestine precipitation results in the Sr gradients only providing only a minimum estimate for recrystallization rate.

At both sites, reconstructed water $\delta^{18}O$ values derived using clumped isotopic data showed no significant variation in response to changes in mineralogy (Fig. 13), linear regression indicates an average aragonite end-member value of 1–2‰ relative to SMOW, with a similar value for calcite, this is consistent with measured pore fluid $\delta^{18}O_{water}$ values and surface values (Swart, 2000). From this, it can be inferred that recrystallization at the benthic

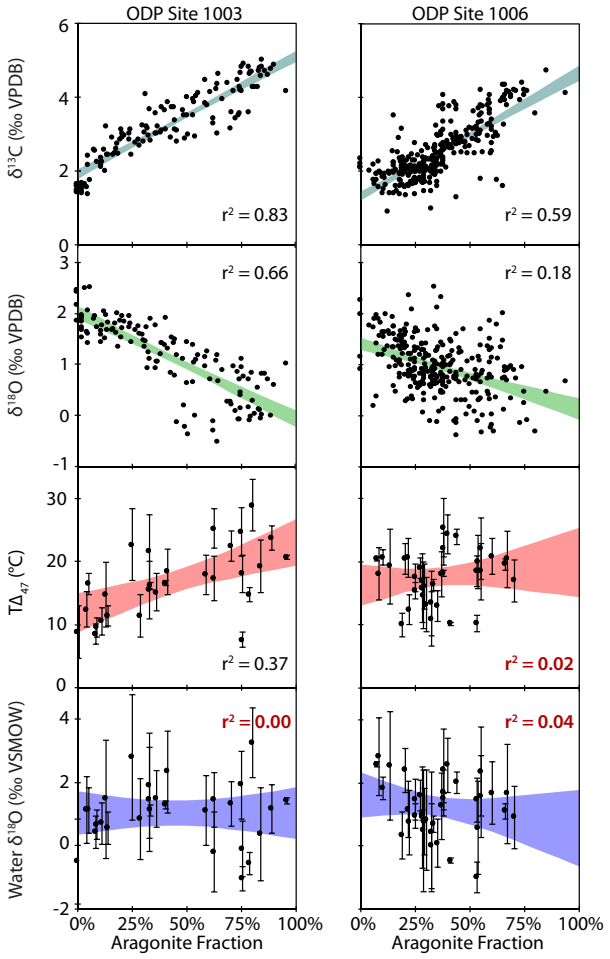

Fig. 13. $\delta^{13}C$, $\delta^{18}O$, $T\Delta_{47}$ and reconstructed water $\delta^{18}O$ values plotted relative to aragonite abundance for the upper 200 mbsf of ODP Sites 1003 and 1006. Shaded regions delineate ±95% confidence for linear regression. Crossplots where $p > 0.05$ for linear correlations' r^2 values are bolded in red. Mineralogy and carbon isotopic data from Swart and Eberli,(2005). (For interpretation of the references to color in this figure legend, the reader is referred to the web version of this article.)

temperature is the driving factor in governing the observed trend toward more positive $\delta^{18}O$ values, rather than a change in fluid composition.

The uppermost $\delta^{18}O$ and Δ_{47} values of the sediments illustrate the plausibility of a diagenetic solution to the "cool tropics paradox" (D'Hondt and Arthur, 1996) wherein the $\delta^{18}O$ values of tropical sediments' record cooler temperatures than those predicted by climate models. Sediments recrystallizing at benthic temperatures during early burial will record this cooler benthic temperature in their isotopic composition, overprinting warmer surface temperatures (Bernard et al., 2017; Schrag, 1999), this effect has been observed in foraminifera via the analyses of diagenetic overgrowths and primary material (Kozdon et al., 2011). This effect would be expected to be most pronounced at lower latitudes where the vertical ocean temperature gradient is greatest. These apparently cooler equatorial temperatures have, however, also been observed in terrestrial biota phosphate $\delta^{18}O$ values (Amiot et al., 2004), which would not be affected by marine diagenesis; this would imply that the "cool tropics" effect is either primary, or that some separate process has also worked to dampen the latitudinal temperature gradient in terrestrial records.

The sediments analyzed in this study present an extreme example of early burial alteration where sediments undergo rapid diagenesis, likely driven by the neomorphism of aragonite to calcite. This rapid re-equilibration at the seafloor, and during early burial in the flushed zone, allows many geochemical proxies to be modified in essentially an open system (Ahm et al., 2018), allowing robust rock buffered isotopic systems (e.g. carbon and calcium) to be overprinted to a significant degree.

4.2. Deeper burial: co-evolving sediments and pore fluids in a closed system

Sites 1003 and 1006 show substantially different downcore trends in $\delta^{18}O$ and $T\Delta_{47}$ values. Site 1003 reports progressively warmer $T\Delta_{47}$ values and more positive fluid $\delta^{18}O$ values below 200 mbsf, whereas Site 1006 shows no significant variance below this depth. This behavior is illustrated in Fig. 14 using a correlated error plot, which delineates a region of temperature and fluid $\delta^{18}O$ values for each sample. This figure is created by parametrically defining an ellipse for each sample where the axes represent the uncertainty of $\delta^{18}O$ measurements and the uncertainty of Δ_{47} measurements, and then transforming each point on that ellipse into temperature and fluid $\delta^{18}O$ values. This was adapted from the approach used by Cummins et al. (2014) such that mixed-mineralogy samples could be plotted. The color of each ellipse represents the carbonate mineralogy determined using XRD, a MATLAB™ script is provided as supplementary material which can be used to produce similar figures. These figures illustrate that the primary source of uncertainty in reconstructing fluid $\delta^{18}O$ values is the uncertainty of $T\Delta_{47}$, rather than carbonate $\delta^{18}O$ values. Because of this, the region delineating the uncertainty in estimates of crystallization temperature and fluid $\delta^{18}O$ values is at an angle, defined by the temperature-dependence of the fractionation factor.

Both sites trend towards more positive carbonate $\delta^{18}O$ values and cooler $T\Delta_{47}$ values in their uppermost sediments (Figs. 7 and 8). This co-varies significantly with transition from aragonite to calcite at Site 1003, and is less significantly correlated at Site 1006 (Fig. 13). The observed change in carbonate $\delta^{18}O$ values is largely due to a change in crystallization temperature although there is a trend towards more negative fluid $\delta^{18}O$ values at Site 1006 (Fig. 14a). Site 1003, in contrast, does not show a significant a change in reconstructed fluid $\delta^{18}O$ in the uppermost sediments (Fig. 14b). More deeply buried sediments at these two sites illustrate very different behaviors, Site 1006 shows little change downcore below 200 mbsf in either temperature or $\delta^{18}O$ values (Fig. 14c). Site 1003 shows a significant increase in reconstructed $\delta^{18}O$ values below this depth, which can be attributed to a combination of warmer crystallization temperatures and more enriched fluid $\delta^{18}O$ values (Fig. 14d). These results suggest that the uppermost

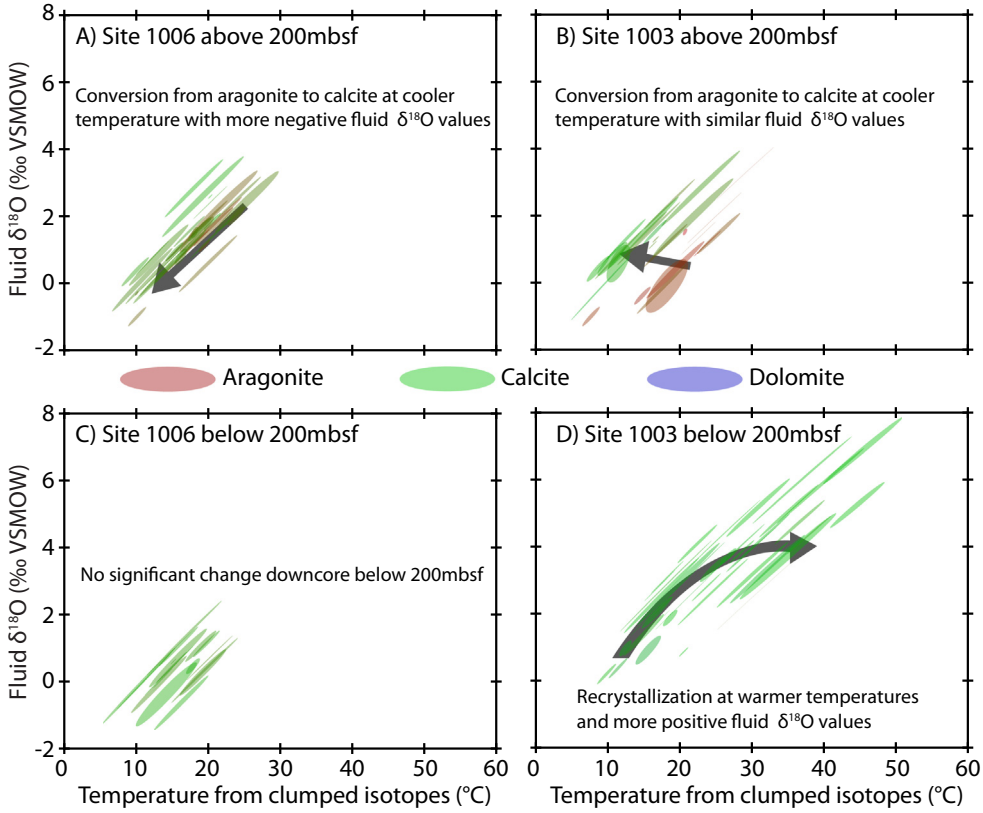

Fig. 14. Correlated uncertainty diagram (ellipses delineate ± 1 s.e. of mean) for $T\Delta_{47}$ and reconstructed fluid $\delta^{18}O$ values for (A) Site 1006, upper 200 mbsf, (B) Site 1003, upper 200 mbsf, (C) Site 1006 deeper sediments and (D) Site 1003 deeper sediments.

sediments at both sites are characterized by an open-system diagenetic behavior with respect to oxygen isotopes, where sediments recrystallize at the cool benthic temperature in an essentially unmodified seawater; and deeper sediments at Site 1003 continue to recrystallize in more diffusively limited communication with seawater which facilitates the modification of pore fluid $\delta^{18}O$ values via reaction with carbonate.

At Site 1003, the bulk carbonate $\delta^{18}O$ values continue to become more positive until the mid-Miocene while Site 1006 trends towards more negative values before 2.6 Ma, below which there is no statistically significant change (Fig. 15). Temperatures recorded in clumped isotope distributions give similar values for both sites until the mid-Miocene (12 Ma) below which, Site 1003 begins to record warmer temperatures which coincides with a trend towards more negative $\delta^{18}O$ values, and with a period of enhanced deposition at this site.

Unlike the uppermost 200 mbsf, the changes in $\delta^{18}O$ values at Site 1003 appear to be driven by both changes in temperature and in fluid $\delta^{18}O$ values (Fig. 14b). Reconstructed fluid $\delta^{18}O$ values begin to differ significantly between the two sites at approximately 5 Ma (Fig. 15). This difference in downcore porefluid $\delta^{18}O$ values has been observed directly at these two sites (Swart, 2000), which show a pronounced increase in $\delta^{18}O$ values at Site 1003 (Fig. 8), with no significant downcore changes at Site 1006 (Fig. 7). The differences in sediment accumulation rate, as well as the significant difference in the age of the oldest sediments at each site, raises the question of whether the observed differences in isotopic composition are simply due to these factors. This question is addressed using time integrated models in the following section. By simulating the burial history of materials with the same reactive properties using the sediment accumulation model for Site 1006, it can be determined whether the observed differences are merely due to differences in depositional history, or due to fundamental differences in the reactivity of the emplaced sediments.

The underlying mechanism driving the difference in rate of burial recrystallization remains enigmatic. Previous workers (Kramer et al., 2000; Swart 2000)). have argued that this may be related to the abundant pyrite at Site 1006, absent at Site 1003 above 1040 mbsf. At Site 1006 the sediments contain higher concentrations of Fe related to the erosion of sediments from Cuba. Reaction of Fe with hydrogen sulfide forming pyrite, limits the decrease in pH at this site and subsequent diagenesis.

The absolute value for fluid $\delta^{18}O$ values reconstructed using clumped isotopes exceeds the measured fluid $\delta^{18}O$ values at Site 1003 at approximately 500 mbsf (Fig. 8). A fraction of this discrepancy may be a result of rate-dependent oxygen isotope fractionation, slowly precipitating calcites have been observed to deviate by over 1‰ from synthetic $\delta^{18}O$ calibrations (Kluge et al., 2014). This difference in fractionation factors could account for up to half of this observed trend. The maximum porefluid $\delta^{18}O$ value at

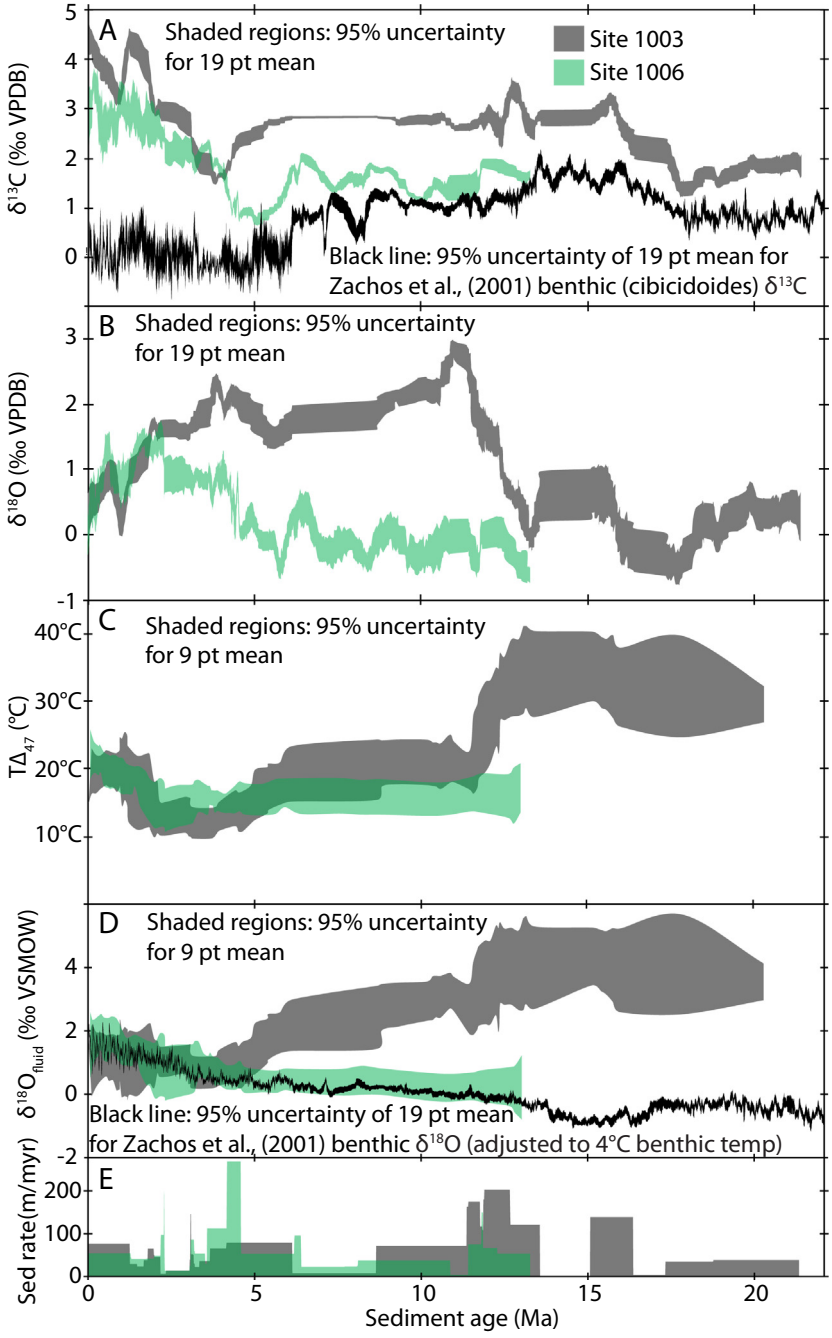

Fig. 15. (A) $\delta^{13}C$ values, (B) $\delta^{18}O$ values, (C) $T\Delta_{47}$ values, (D) reconstructed fluid $\delta^{18}O$ values and (E) sedimentation rate for Sites 1003 (Grey shaded region) and 1006 (Green shaded region) plotted relative to sediment age. Zachos et al. (2001) benthic $\delta^{18}O$ values adjusted to seawater $\delta^{18}O$ values assuming a benthic temperature of 4 °C. Shaded regions correspond to ± 95% confidence intervals shown in previous figures.

present is approximately 3‰ V-SMOW, however, the reconstructed $\delta^{18}O_{fluid}$ value for sediments deposited prior to 13 Ma ranged between 3‰ and 5‰. It is possible that the observed pore fluid $\delta^{18}O$ gradients have not been constant over time, and may have previously been more positive in value during the past at Site 1003, this possibility was investigated using time-integrated modeling, discussed in Sections 4.3 and 4.4 of this manuscript.

4.3. Comparison between time-integrated models and measured values

The difference in $\delta^{18}O$ and Δ_{47} values between Sites 1003 and 1006 cannot be accounted for simply by differences in sediment accumulation history for the two sites. Nor is the difference simply due to variable supply of the pelagic and platform derived sediment end members. The two sites

differ fundamentally from one another with respect to long-term sediment reactivity. This is illustrated in the results of time-integrated models where no single set of sediment reactivity coefficients can describe both sites' isotopic compositions. Models which best describe Site 1003 remain reactive during deeper burial and are accompanied with an enhanced degree of fluid/rock coevolution of oxygen isotopes. Models which best describe Site 1006 undergo the same initial rapid recrystallization as at Site 1003, however, these sediments are then comparatively stable ($\beta = 0.5, 0.1$) when compared to the platform proximal site.

All models simulated an initially rapid rate of recrystallization (Fig. 6), the trend towards cooler $T\Delta_{47}$ values in the uppermost sediments accurately described by all models (Fig. 9a). The observed trend in measured values towards warmer temperatures downcore required diagenetic carbonates to continue recrystallizing at a similar rate to primary materials. Models where diagenetic material was only 10% as reactive ($\beta = 0.1$) gave consistently cooler values when compared to measured values; this behavior best describes the measured data from Site 1006, but not for Site 1003. Models where sediments constantly undergo diagenesis, however, result in the warmest temperatures at depth and are nearly parallel to, albeit offset from, the present geothermal gradient. This is different from the measured behavior at Site 1003, where measured carbonate $T\Delta_{47}$ values in the sediment appear to show little change downcore below a depth of 700 mbsf at Site 1003. Models where sediments become less reactive over time, but are free to continue recrystallizing even after initial diagenesis ($\beta = 1.0$, 0.5) (red and green solid lines in Fig. 9) give the best approximation of this behavior, and the apparently best-fitting model simulates for Site 1003 an exponential decrease in reaction rate to zero, with a half-life of 7.2 myr ($C = 5$ myr, $\beta = 1.0$). The initial recrystallization rate of the "pulse + constant" model was slower than the initial recrystallization rates of the other two models (Fig. 6), and better approximated the trend towards cooler values in the uppermost sediments at Site 1006. The more deeply buried $T\Delta_{47}$ values for Site 1006 were best fit by modelling authigenic materials as less reactive compared to primary material (Fig. 10).

In models where the present-day downcore gradient in porewater $\delta^{18}O$ values was assumed to be constant throughout time, irrespective of recrystallization history, these models failed to produce results comparable to the measured values below a depth of 400 mbsf (Fig. 9b). Models where the porewater $\delta^{18}O$ gradient was double in the early Miocene and then decreased to its present composition between 10 Ma and the present day better approximated the observed trend in reconstructed fluid composition from clumped isotopes and $\delta^{18}O$ values. Like the reconstructed temperatures, the best-fit models simulated a decrease in recrystallization rate over time, as constantly recrystallizing sediments equilibrate to the present pore fluid composition. The best-fit model for both reconstructed water $\delta^{18}O$ and $T\Delta_{47}$ values simulated an exponential decrease in reaction rate to zero (blue line), where diagenetically altered material is as reactive as primary material, although becoming more stable with time.

These time-integrated depositional models made no assumption regarding the origin of the downcore gradient pore fluid $\delta^{18}O$ values. However, the models which most closely approximate measured values at Site 1003 suggest that the pore fluid gradient could have been more positive in the past. Possible explanations for this are discussed in the following section.

4.4. Origin of downcore gradients in $\delta^{18}O$ values and implications for seawater $\delta^{18}O$ reconstructions

It has been argued that the observed gradient in $\delta^{18}O$ values can be ostensibly explained by carbonate recrystallization (Swart, 2000), although several other possibilities exist. Such possibilities include lateral migration of evaporative brines, or upward diffusion of a deeper fluid. Covariation between more positive $\delta^{18}O$ values and the observed increase in chloride concentration at depth could be interpreted as being the result of lateral migration of evaporative brines from the platform. This lateral migration would require significant formation of evaporative brines on GBB during previous sea-level highstands, which are subsequently transported to considerable depth and distance from the margin. However, the lack of correlation between $\delta^{2}H$ and $\delta^{18}O$ values in the fluids measured by Swart (2000) precludes an exclusively evaporative origin for these fluids, however. While at Site 1003, the concentration of Cl^{-} increases downcore from 570 mM to 1000 mM, correlating with the increase in $\delta^{18}O$ value, Site 1006 the increases in chloride shows no correlation with fluid $\delta^{18}O$ values (Swart, 2000).

The increase in salinity/chlorinity downcore may be unrelated to the $\delta^{18}O$ variation, as dissolution of Cretaceous-aged evaporites (Schlager et al., 1988; Schlager and Ginsburg, 1981) could produce such a gradient; analyses of a similar system on the New Jersey margin showed no covariation between chlorinity and $\delta^{18}O$ values (van Geldern et al., 2013). The dissolution of halite would, however, result in a trend in pore fluids towards a 1:1 molar ratio of sodium to chloride as chlorinity increases. This is not observed in the fluids, which maintain a consistent Na/Cl ratio of 0.85 downcore (Kramer et al., 2000). Biogenic carbonates, such as echinoderm HMC, incorporate elevated concentrations of sodium and chloride within their skeleton (Harriss and Pilkey, 1966); similarly, aragonite will incorporate a greater amount of sodium and chloride than calcite (Land and Hoops, 1973). Kramer et al. (2000) suggest that the dissolution of these metastable primary materials and subsequent precipitation of authigenic calcite (and trace dolomite) would result in the expulsion of sodium and chloride. A simple mass balance by Kramer et al. (2000) calculates that the neomorphism of 25% of these metastable minerals can account for the observed increase in sodium and chloride abundance as well as the observed changes in water $\delta^{18}O$ values. This process was described by Malone et al. (1990) during ODP Leg 115 in the Maldives. The clumped isotope method readily reconstructs paleofluid $\delta^{18}O$ values, however the salinity and $\delta^{2}H$ values of the Miocene-aged diagenetic fluids remains enigmatic. It is therefore possible that an entirely different mechanism

was responsible for the elevated Miocene porefluid $\delta^{18}O$ values, which cannot be unambiguously constrained using the available data.

Several scenarios could have resulted in the formation of fluids with more positive $\delta^{18}O$ values, such as enhanced migration of evaporative fluids from the bank top as well as more closed-system diagenetic behavior. The increased rate of sediment accumulation during the early Miocene (Fig. 15e) could result in more closed-system diagenetic behavior of oxygen isotopes as has been observed in calcium isotope values. Differences in mineral precipitation rates can result in different degrees of oxygen isotope fractionation, (Watkins et al., 2014). It is possible that some of the observed trend is due to recrystallization occurring at a slower rate during deeper burial. It is difficult to constrain the precise rate at which the chemical reactions occurred, however if the "Equilibrium Limit" for oxygen isotope fractionation proposed by Watkins et al. is used, around half of the observed difference can be accounted for.

The extent of water/rock interaction can be estimated using the clumped isotope and $\delta^{18}O$ values presented in this manuscript. A water – rock coevolution model for sediments buried below 200 mbsf ($\delta^{18}O_{carbonate} = +2.0‰$, $\delta^{18}O_{fluid} = +1.0‰$) is shown in Fig. 16a, which simulates different water/rock (W/R) ratios. This approach is derived from Ryb and Eiler (2018). Clumped isotope measurements of the deeper sediments at Site 1003 indicate a median W/R ratio of 0.61 for oxygen, which corresponds to a calcium carbonate unit with a porosity of 0.53 (Fig. 16b). These results are similar to more deeply buried calcite and dolomite sediments recovered in the Andros core, analyzed by Winkelstern and Lohmann (2016), which fall along a trend corresponding to a median W/R ratio of 0.96 (porosity = 0.66, dolomite) (Fig. 16c and d). Analyses of authigenic dolomites by Ryb and Eiler (2018) successfully replicate the familiar variation in carbonate $\delta^{18}O$ values over the Phanerozoic (Veizer et al., 1999; Veizer and Prokoph, 2015); clumped isotope measurements of these Phanerozoic dolomites demonstrate a similar behavior to that described in the Bahamas by Winkelstern and Lohmann (2016) and in this study, wherein warmer temperatures are accompanied by more negative bulk $\delta^{18}O$ values, but nevertheless formed from fluids with more positive $\delta^{18}O$ values. Other dolomites from the same dataset reconstruct less rock-buffered $\delta^{18}O$ values, indicating some may have formed at high temperatures but from relatively unmodified seawater (Fig. 16e). Calculations of the W/R ratio for these Phanerozoic dolomites using the clumped isotope measurements yield a median value of 1.58 (Fig. 16f), which results in a relatively high estimate of porosity for a purely closed system of 0.76. The estimated porosity for these three datasets is modeled for a purely closed system, however it is likely that over millions of years oxygen exchanged with an outside system. These three datasets illustrate essentially the same behavior from early to late burial, where fluids and sediments co-evolve at increasing burial temperatures with limited exchange of water with external sources.

Analyses of $\delta^{44/40}Ca$ values of carbonate sediments at Site 1003 by Higgins et al. (2018), give independent evidence for enhanced closed-system recrystallization within

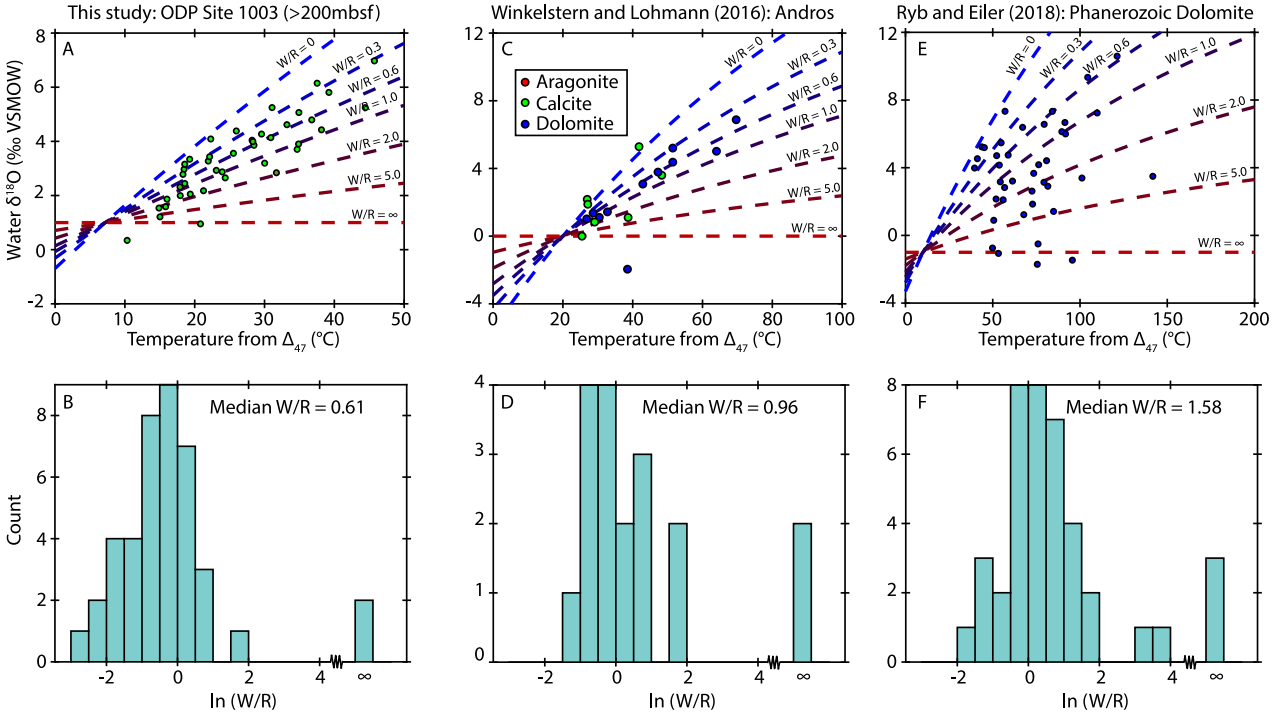

Fig. 16. $T\Delta_{47}$ values plotted relative to reconstructed fluid $\delta^{18}O$ values and histogram plotting frequency of estimated water/rock ratios (W/R). Data shown from This study: ODP Site 1003 (>200 mbsf) (A and B); Winkelstern and Lohmann (2016): Andros Core (C and D); and Ryb and Eiler (2018) Phanerozoic dolomites (E and F). $T\Delta_{47}$ values and interpreted fluid $\delta^{18}O$ values are taken from the respective publications.

the of deeply buried sediments at Site 1003, as the most shallowly buried sediments are apparently altered by diagenetic exchange with seawater, and more deeply buried sediments have less evidence for this exchange (Ahm et al., 2018). This independent proxy for open and closed system diagenesis, combined with the evidence from clumped isotopes for recrystallization at warmer burial temperatures, suggest that the more deeply buried sediments at Site 1003 underwent recrystallization with limited seawater exchange resulting in the observed co-evolution of oxygen isotopes between porewater and carbonates.

The trend towards more negative reconstructed water $\delta^{18}O$ values at Site 1006 can be largely attributed to the evolution of Cenozoic seawater $\delta^{18}O$ values. Values reconstructed using clumped isotopes are similar to reconstructed water $\delta^{18}O$ values for the benthic foraminiferal record through the mid-Miocene (Zachos et al., 2001), which have been corrected to a benthic temperature of 4 °C, using Kim and O'Neil (1997)'s temperature relationship (Fig. 15). These values are more positive in the present than during the early Pliocene and Miocene (Lisiecki and Raymo, 2005; Zachos et al., 2001) responding to changes in global ice volume (Emiliani, 1966; Shackleton and Opdyke, 1973). The platform distal Site 1006 preserves these oxygen isotope ratios largely due to the rapid open-system recrystallization followed by no subsequent recrystallization during deeper burial (Fig. 10).

5. CONCLUSION

The sediments recovered from ODP Sites 1003 and 1006 demonstrate that different behaviors of sediment recrystallization/neomorphism can be thermally constrained using the clumped isotope proxy. Results show that Bahamian periplatform sediments undergo rapid diagenesis during early burial, a process likely driven by the neomorphism of aragonite to calcite. This is illustrated at Site 1003 by a significant linear co-variation between $T\Delta_{47}$ and the abundance of aragonite, suggesting that the LMC endmember formed predominantly at or near the benthic temperature. This covariation with mineralogy has also been observed in carbon, oxygen, and calcium isotope ratios, suggesting some degree of open-system recrystallization in addition to the sediment mixing model previously described at this site. Site 1006 shows less covariance between mineralogy and the temperature-sensitive $\delta^{18}O$ and Δ_{47} proxies, indicating that the sediment heterogeneity at the deeper site may be reflecting variation in the supply of pelagic and platform-derived end-members over glacial-interglacial cycles. Recrystallization of sediments during deeper burial can result in significant modification of pore fluid $\delta^{18}O$ values. At Site 1003, this change in fluid $\delta^{18}O$ values, as well as recrystallization in the geothermal gradient, can be observed using the clumped isotope measurements. The observed pattern of water-rock coevolution of oxygen isotopes at Site 1003 is similar to observed behaviors in other deep cores, as well as authigenic dolomites from throughout the Phanerozoic. Reconstructed oxygen isotope values suggest that the pore fluids were more positive during the Miocene than at present day, possibly because of faster burial rates during the mid-Miocene which resulted in less diffusive exchange with seawater. Some of these more positive reconstructed fluid $\delta^{18}O$ values in the Miocene may also be due to differences in rate-dependent fractionation of oxygen isotopes during slower authigenic calcite precipitation. Site 1006, which does not have such as significant modern variation in pore fluid $\delta^{18}O$ values, also shows little to no variation in reconstructed water $\delta^{18}O$ values, with fluid compositions reconstructed using clumped isotopes largely agreeing with secular change in Cenozoic global seawater $\delta^{18}O$ values.

ACKNOWLEDGMENTS

This research was made possible through funding from the Petroleum Research Fund Grant #AC-52863ND2 and from NSF grant OCE-1635874 to PKS. The Thermo-253 was acquired using funding from NSF grant EAR-0926503 to PKS. The salary of PTS was partially supported by the 2016 Schlanger Fellowship from the US Science Support Program. Chris Kaiser is acknowledged for his technical support with XRD. The paper benefited from the reviews of two anonymous reviewers and the editorial comments of Greta Mackenzie.

APPENDIX A. SUPPLEMENTARY MATERIAL

Supplementary data to this article can be found online at https://doi.org/10.1016/j.gca.2019.05.002.

REFERENCES

Adkins J. F. and Schrag D. P. (2003) Reconstructing Last Glacial Maximum bottom water salinities from deep-sea sediment pore fluid profiles. *Earth Planet. Sci. Lett.* **216**, 109–123.

Ahm A.-S. C., Bjerrum C. J., Blättler C. L., Swart P. K. and Higgins J. A. (2018) Quantifying early marine diagenesis in shallow-water carbonate sediments. *Geochimica et Cosmochimica Acta*.

Amiot R., Lécuyer C., Buffetaut E., Fluteau F., Legendre S. and Martineau F. (2004) Latitudinal temperature gradient during the Cretaceous Upper Campanian-Middle Maastrichtian: $\delta^{18}O$ record of continental vertebrates. *Earth Planet. Sci. Lett.* **226**, 255–272.

Anselmetti F. S., Eberli G. P. and Ding Z.-D. (2000) From the Great Bahama Bank into the Straits of Florida: a margin architecture controlled by sea-level fluctuations and ocean currents. *Geol. Soc. Am. Bull.* **112**, 829–844.

Baker P. A., Gieskes J. M. and Elderfield H. (1982) Diagenesis of carbonates in deep-sea sediments-evidence from Sr/Ca ratios and interstitial dissolved Sr^{2+} data. *J. Sediment. Petrol.* **52**, 071–082.

Bernard S., Daval D., Ackerer P., Pont S. and Meibom A. (2017) Burial-induced oxygen-isotope re-equilibration of fossil foraminifera explains ocean paleotemperature paradoxes. *Nat. Commun.* **8**, 1134.

Berner R. A. (1980) *Early Diagenesis: A Theoretical Approach*. Princeton University Press.

Betzler C., Reijmer J. J. G., Bernet K., Eberli G. P. and Anselmetti F. S. (1999) Sedimentary patterns and geometries of the Bahamian outer carbonate ramp (Miocene-Lower Pliocene, Great Bahama Bank). *Sedimentology* **46**, 1127–1143.

Bischoff J. L. and Fyfe W. (1968) Catalysis, inhibition, and the calcite-aragonite problem; [Part] 1, The aragonite-calcite transformation. *Am. J. Sci.* **266**, 65–79.

Boardman M. R. and Neumann A. C. (1984) Sources of periplatform carbonates: northwest Providence Channel, Bahamas. *J. Sediment. Res.* **54**, 1110–1123.

Cloud P. E. (1962) *Environment of calcium carbonate deposition west of Andros Island, Bahamas* U.S. Geological Survey Professional Papers. US Govt. Print. Off., pp. 1–138.

Compton J. S. and Siever R. (1986) Diffusion and mass balance of Mg during early dolomite formation, Monterey Formation. *Geochimica et Cosmochimica Acta* **50**, 125–135.

Craig H. (1957) Isotopic standards for carbon and oxygen and correction factors for mass-spectrometric analysis of carbon dioxide. *Geochimica et Cosmochimica Acta* **12**, 133–149.

Cummins R. C., Finnegan S., Fike D. A., Eiler J. M. and Fischer W. W. (2014) Carbonate clumped isotope constraints on Silurian ocean temperature and seawater $\delta^{18}O$. *Geochimica et Cosmochimica Acta* **140**, 241–258.

D'Hondt S. and Arthur M. A. (1996) Late Cretaceous oceans and the cool tropic paradox. *Science* **271**, 1838–1841.

Daëron M., Blamart D., Peral M. and Affek H. P. (2016) Absolute isotopic abundance ratios and the accuracy of Δ_{47} measurements. *Chem. Geol.* **442**, 83–96.

Defliese W. F. and Lohmann K. C. (2016) Evaluation of meteoric calcite cements as a proxy material for mass-47 clumped isotope thermometry. *Geochimica et Cosmochimica Acta* **173**, 126–141.

Dennis K. J., Affek H. P., Passey B. H., Schrag D. P. and Eiler J. M. (2011) Defining an absolute reference frame for 'clumped' isotope studies of CO_2. *Geochimica et Cosmochimica Acta* **75**, 7117–7131.

Eberli G., Swart P. and Malone M., et al. (1997a) Proceedings of the Ocean Drilling Program. *Ocean Drilling Program* **Vol. 166**, Initial Reports, Bahamas Transect.

Eberli G. P., Anselmetti F. S., Kroon D., Sato T. and Wright J. D. (2002) The chronostratigraphic significance of seismic reflections along the Bahamas Transect. *Mar. Geol.* **185**, 1–17.

Eberli G. P., Swart P. K., McNeill D. F., Kenter J. A. M., Anselmetti F. S., Melim L. A. and Ginsburg R. N. (1997b) A synopsis of the Bahamas Drilling Project: Results from two deep core borings drilled on the Great Bahama bank. In *Proceedings of the Ocean Drilling Program, Initial Reports 166*, pp. 23–41.

Eiler J. M. (2011) Paleoclimate reconstruction using carbonate clumped isotope thermometry. *Quat. Sci. Rev.* **30**, 3575–3588.

Emiliani C. (1966) Paleotemperature analysis of carribean cores P6304–8 and P6304–9 and a generalized temperature curve for the past 425,000 years. *J. Geol.* **74**, 109–124.

Fantle M. S. and DePaolo D. J. (2007) Ca isotopes in carbonate sediment and pore fluid from ODP Site 807A: The Ca^{2+} (aq)–calcite equilibrium fractionation factor and calcite recrystallization rates in Pleistocene sediments. *Geochimica et Cosmochimica Acta* **71**, 2524–2546.

Folk R. L. (1965) *Some Aspects of Recrystallization in Ancient Limestones*. Society for Economic Paleontologists and Mineralogists Dolomitization and Limestone Diagenesis (SP13).

Ghosh P., Adkins J., Affek H., Balta B., Guo W., Schauble E. A., Schrag D. and Eiler J. M. (2006) ^{13}C–^{18}O bonds in carbonate minerals: A new kind of paleothermometer. *Geochimica et Cosmochimica Acta* **70**, 1439–1456.

Ginsburg, R.N., 2001. Subsurface geology of a prograding carbonate platform margin, Great Bahama Bank: results of the Bahamas Drilling Project.

Guo Y., Deng W. and Wei G. (2019) Kinetic effects during the experimental transition of aragonite to calcite in aqueous solution: Insights from clumped and oxygen isotope signatures. *Geochimica et Cosmochimica Acta.*.

Gussone N., Böhm F., Eisenhauer A., Dietzel M., Heuser A., Teichert B. M., Reitner J., Wörheide G. and Dullo W.-C. () Calcium isotope fractionation in calcite and aragonite. *Geochimica et Cosmochimica Acta* **69**, 4485–4494.

Harriss, R.C., Pilkey, O.H., 1966. Temperature and salinity control of the concentration of skeletal Na, Mn, and Fe in Dendraster excentricus.

He B., Olack G. A. and Colman A. S. (2012) Pressure baseline correction and high-precision CO_2 clumped-isotope (Δ_{47}) measurements in bellows and micro-volume modes. *Rapid Commun. Mass Spectrom.: RCM* **26**, 2837–2853.

Henderson G. M., Slowey N. C. and Haddad G. A. (1999) Fluid flow through carbonate platforms: constraints from 234 U/238 U and Cl^- in Bahamas pore-waters. *Earth Planet. Sci. Lett.* **169**, 99–111.

Higgins J. A., Blättler C. L., Lundstrom E. A., Santiago-Ramos D. P., Akhtar A. A., Crüger Ahm A. S., Bialik O., Holmden C., Bradbury H., Murray S. T. and Swart P. K. (2018) Mineralogy, early marine diagenesis, and the chemistry of shallow-water carbonate sediments. *Geochimica et Cosmochimica Acta* **220**, 512–534.

Huntington K. W., Budd D. A., Wernicke B. P. and Eiler J. M. (2011) Use of clumped-isotope thermometry to constrain the crystallization temperature of diagenetic calcite. *J. Sediment. Res.* **81**, 656–669.

Huntington K. W., Eiler J. M., Affek H. P., Guo W., Bonifacie M., Yeung L. Y., Thiagarajan N., Passey B., Tripati A., Daeron M. and Came R. (2009) Methods and limitations of 'clumped' CO_2 isotope (Δ_{47}) analysis by gas-source isotope ratio mass spectrometry. *J. Mass Spectrom.* **44**, 1318–1329.

Immenhauser A., Kenter J. A., Ganssen G., Bahamonde J. R., Van Vliet A. and Saher M. H. (2002) Origin and significance of isotope shifts in Pennsylvanian carbonates (Asturias, NW Spain). *J. Sediment. Res.* **72**, 82–94.

Jones D. S., Creel R. C., Rios B. and Santiago Ramos D. P. (2015) Chemostratigraphy of an Ordovician-Silurian carbonate platform: $\delta^{13}C$ records below glacioeustatic exposure surfaces. *Geology* **43**, 59–62.

Katz A., Sass E., Starinsky A. and Holland H. (1972) Strontium behavior in the aragonite-calcite transformation: an experimental study at 40–98 C. *Geochimica et Cosmochimica Acta* **36**, 481–496.

Kim S.-T. and O'Neil J. R. (1997) Equilibrium and nonequilibrium oxygen isotope effects in synthetic carbonates. *Geochimica et Cosmochimica Acta* **16**, 3461–3475.

Kim S.-T., O'Neil J. R., Hillaire-Marcel C. and Mucci A. (2007) Oxygen isotope fractionation between synthetic aragonite and water: Influence of temperature and Mg^{2+} concentration. *Geochimica et Cosmochimica Acta* **71**, 4704–4715.

Kluge T., Affek H. P., Dublyansky Y. and Spötl C. (2014) Devils Hole paleotemperatures and implications for oxygen isotope equilibrium fractionation. *Earth Planet. Sci. Lett.* **400**, 251–260.

Kozdon R., Kelly D. C., Kita N. T., Fournelle J. H. and Valley J. W. (2011) Planktonic foraminiferal oxygen isotope analysis by ion microprobe technique suggests warm tropical sea surface temperatures during the Early Paleogene. *Paleoceanography* **26**, 1–17.

Kramer P. A., Swart P. K., Carlo E. H. D. and Schovsbo N. H. (2000) Overview of interstitial fluid and sediment geochemistry, Sites 1003–1007 (Bahamas transect). *Proceedings of the Ocean Drilling Program, Scientific Results* **166**, 179–195.

Land L. S. and Hoops G. K. (1973) Sodium in carbonate sediments and rocks: a possible index to the salinity of diagenetic solutions. *J. Sediment. Res.*, 43.

Lasemi Z. and Sandberg P. A. (1984) Transformation of aragonite-dominated lime muds to microcrystalline limestones. *Geology* **12**, 420–423.

Leaman K. D., Vertes P. S., Atkinson L. P., Lee T. N., Hamilton P. and Waddell E. (1995) Transport, potential vorticity, and

current/temperature structure across Northwest Providence and Santaren Channels and the Florida Current off Cay Sal Bank. *J. Geophys. Res.: Oceans* **100**, 8561–8569.

Lemarchand D., Wasserburg G. and Papanastassiou D. (2004) Rate-controlled calcium isotope fractionation in synthetic calcite. *Geochimica et Cosmochimica Acta* **68**, 4665–4678.

Lisiecki L. E. and Raymo M. E. (2005) A Pliocene-Pleistocene stack of 57 globally distributed benthic $\delta^{18}O$ records. *Paleoceanography* **20**, n/a–n/a.

Lowenstam H. A. and Epstein S. (1957) On the origin of sedimentary aragonite needles of the Great Bahama Bank. *J. Geol.* **65**, 364–375.

Loyd S. J., Sample J., Tripati R. E., Defliese W. F., Brooks K., Hovland M., Torres M., Marlow J., Hancock L. G., Martin R., Lyons T. and Tripati A. E. (2016) Methane seep carbonates yield clumped isotope signatures out of equilibrium with formation temperatures. *Nat. Commun.* **7**, 12274.

Lüdmann T., Paulat M., Betzler C., Möbius J., Lindhorst S., Wunsch M. and Eberli G. P. (2016) Carbonate mounds in the Santaren Channel, Bahamas: a current-dominated periplatform depositional regime. *Mar. Geol.* **376**, 69–85.

Malone M. J., Baker P. A., Burns S. J. and Swart P. K. (1990) Geochemistry of periplatform carbonate sediments, Leg 115, Site 716 (Maldives Archipelago, Indian Ocean). In *Proceedings of the Ocean Drilling Program, Scientific Results. Ocean Drilling Program*, pp. 647–659.

Mangenot X., Bonifacie M., Gasparrini M., Götz A., Chaduteau C., Ader M. and Rouchon V. (2017) Coupling Δ_{47} and fluid inclusion thermometry on carbonate cements to precisely reconstruct the temperature, salinity and $\delta^{18}O$ of paleogroundwater in sedimentary basins. *Chem. Geol.* **472**, 44–57.

Matthews A. and Katz A. (1977) Oxygen isotope fractionation during the dolomitization of calcium carbonate. *Geochimica et Cosmochimica Acta* **41**, 1431–1438.

Murray S. T., Arienzo M. M. and Swart P. K. (2016) Determining the Δ_{47} acid fractionation in dolomites. *Geochimica et Cosmochimica Acta* **174**, 42–53.

Passey B. H., Levin N. E., Cerling T. E., Brown F. H. and Eiler J. M. (2010) High-temperature environments of human evolution in East Africa based on bond ordering in paleosol carbonates. *Proc. National Acad. Sci. USA* **107**, 11245–11249.

Purdy E. G. (1963a) Recent calcium carbonate facies of the Great Bahama Bank. 1. Petrography and reaction groups. *J. Geol.* **71**, 334–355.

Purdy E. G. (1963b) Recent calcium carbonate facies of the Great Bahama Bank. 2. Sedimentary facies. *J. Geol.* **71**, 472–497.

Reijmer J. J., Swart P. K., Bauch T., Otto R., Reuning L., Roth S. and Zechel S. (2009) A re-evaluation of facies on Great Bahama Bank I: new facies maps of western Great Bahama Bank. In *Perspect Carbonate Geol A Tribute Career Robert Nathan Ginsburg (Spec Publ 41 IAS)*, 98, pp. 29–46. Perspect Carbonate Geol A Tribute Career Robert Nathan Ginsburg (Spec Publ 41 IAS).

Richter F. M. and DePaolo D. J. (1987) Numerical models for diagenesis and the Neogene Sr isotopic evolution of seawater from DSDP Site 590B. *Earth Planet. Sci. Lett.* **83**, 27–38.

Ryb U. and Eiler J. M. (2018) Oxygen isotope composition of the Phanerozoic ocean and a possible solution to the dolomite problem. *Proc. National Acad. Sci. USA* **115**, 6602–6607.

Schauble E. A., Ghosh P. and Eiler J. M. (2006) Preferential formation of ^{13}C–^{18}O bonds in carbonate minerals, estimated using first-principles lattice dynamics. *Geochimica et Cosmochimica Acta* **70**, 2510–2529.

Schlager, W., Bourgeois, F., Mackenzie, G., Smit, J., 1988. Boreholes at Great Isaac and Site 626 and the History of the Florida Straits, Vol. 101.

Schlager W. and Ginsburg R. N. (1981) Bahama carbonate platforms—the deep and the past. *Mar. Geol.* **44**, 1–24.

Schlager W. and James N. (1978) Low-magnesium calcite limestones forming at the deep-sea floor. Tongue of the Ocean, Bahamas. *Sedimentology* **25**, 675–702.

Schrag D. P. (1999) Effects of diagenesis on the isotopic record of late Paleogene tropical sea surface temperatures. *Chem. Geol.* **161**, 215–224.

Schrag D. P., Adkins J. F., McIntyre K., Alexander J. L., Hodell D. A., Charles C. D. and McManus J. F. (2002) The oxygen isotopic composition of seawater during the Last Glacial Maximum. *Quat. Sci. Rev.* **21**, 331–342.

Schrag D. P., DePaolo D. J. and Richter F. M. (1995) Reconstructing past sea surface temperatures: correcting for diagenesis of bulk marine carbonate. *Geochimica et Cosmochimica Acta* **59**, 2265–2278.

Shackleton N. J. and Opdyke N. D. (1973) Oxygen Isotope and Palaeomagnetic Stratigraphy of Equitorial Pacific Core V28–238: Oxygen Isotope Temperature and Ice Volumes on a 10^5 Year and 10^6 Year Scale. *Quatern. Res.* **3**, 39–55.

Skelton P. W. and Gili E. (2012) Rudists and carbonate platforms in the Aptian: a case study on biotic interactions with ocean chemistry and climate. *Sedimentology* **59**, 81–117.

Sorby H. C. (1879) The structure and origin of limestones. *Popular Sci. Rev.* **3**, 134–137.

Staudigel P. T., Murray S., Dunham D. P., Frank T. D., Fielding C. R. and Swart P. K. (2018) Cryogenic brines as diagenetic fluids: Reconstructing the diagenetic history of the Victoria Land Basin using clumped isotopes. *Geochimica et Cosmochimica Acta* **224**, 154–170.

Staudigel P. T. and Swart P. K. (2016) Isotopic behavior during the aragonite-calcite transition: Implications for sample preparation and proxy interpretation. *Chem. Geol.* **442**, 130–138.

Staudigel P. T. and Swart P. K. (2018) A kinetic difference between ^{12}C and ^{13}C-bound oxygen exchange rates results in decoupled $\delta^{18}O$ and Δ_{47} values of equilibrating DIC solutions. *Geochem. Geophys. Geosyst.*.

Stolper D. A., Eiler J. M. and Higgins J. A. (2018) Modeling the effects of diagenesis on carbonate clumped-isotope values in deep- and shallow-water settings. *Geochimica et Cosmochimica Acta*.

Swart P. K. (2000) The oxygen isotopic composition of interstitial waters: evidence for fluid flow and recrystallization in the margin of the Great Bahama Bank. In *Proceedings of the Ocean Drilling Program, Scientific Results*, 166, p. 8. Proceedings of the Ocean Drilling Program, Scientific Results.

Swart P. K. (2015) The geochemistry of carbonate diagenesis: The past, present and future. *Sedimentology* **62**, 1233–1304.

Swart P.K., and Guzikowski M., 1988, Interstitial water chemistry and diagenesis of periplatform sediments from the Bahamas, ODP Leg 101, in J. Austin, and W. Schlager, eds., Proceedings of the Ocean Drilling Program, Scientific Results, v. 101: College Station, Texas, Ocean Drilling Program, p. 363-380.

Swart P. K., Burns S. and Leder J. (1991) Fractionation of the stable isotopes of oxygen and carbon in carbon dioxide during the reaction of calcite with phosphoric acid as a function of temperature and technique. *Chem. Geol.: Isotope Geosci. Sect.* **86**, 89–96.

Swart P. K. and Eberli G. P. (2005) The nature of the $\delta^{13}C$ of periplatform sediments: Implications for stratigraphy and the global carbon cycle. *Sediment. Geol.* **175**, 115–129.

Swart P. K., James N. P., Mallinson D., Malone M. J., Matsuda H. and Simo T. (2003) Data Report: Carbonate Mineralogy of Sites Drilled during Leg 182. *ODP Sci. Results* **182**.

Swart P. K., Reijmer J. J. and Otto R. (2009) A reevaluation of facies on Great Bahama Bank II: variations in the $\delta^{13}C$, $\delta^{18}O$

and mineralogy of surface sediments. *Perspectives in Carbonate Geology: A Tribute to the Career of Robert Nathan Ginsburg*, 47–59.

Taft W. H. (1967) *Modern Carbonate Sediments, Developments in Sedimentology*. Elsevier, pp. 29–50.

Thaler C., Millo C., Ader M., Chaduteau C., Guyot F. and Ménez B. (2017) Disequilibrium $\delta^{18}O$ values in microbial carbonates as a tracer of metabolic production of dissolved inorganic carbon. *Geochimica et Cosmochimica Acta* **199**, 112–129.

van der Kooij B., Immenhauser A., Csoma A., Bahamonde J. and Steuber T. (2009) Spatial geochemistry of a Carboniferous platform-margin-to-basin transect: Balancing environmental and diagenetic factors. *Sediment. Geol.* **219**, 136–150.

van Geldern R., Hayashi T., Böttcher M. E., Mottl M. J., Barth J. A. and Stadler S. (2013) Stable isotope geochemistry of pore waters and marine sediments from the New Jersey shelf: Methane formation and fluid origin. *Geosphere* **9**, 96–112.

Vaughan A. and Dixon E. (1911) The carboniferous succession in gower. *Quart. J. Geol. Soc.* **67**, 477.

Veizer J., Ala D., Azmy K., Bruckschen P., Buhl D., Bruhn F., Carden G. A., Diener A., Ebneth S. and Godderis Y. (1999) $^{87}Sr/^{86}Sr$, $\delta^{13}C$ and $\delta^{18}O$ evolution of Phanerozoic seawater. *Chemi. Geol.* **161**, 59–88.

Veizer J. and Prokoph A. (2015) Temperatures and oxygen isotopic composition of Phanerozoic oceans. *Earth-Sci. Rev.* **146**, 92–104.

Watkins J. M. and Hunt J. D. (2015) A process-based model for non-equilibrium clumped isotope effects in carbonates. *Earth Planet. Sci. Lett.* **432**, 152–165.

Watkins J. M., Hunt J. D., Ryerson F. J. and DePaolo D. J. (2014) The influence of temperature, pH, and growth rate on the $\delta^{18}O$ composition of inorganically precipitated calcite. *Earth Planet. Sci. Lett.* **404**, 332–343.

Winkelstern I. Z. and Lohmann K. C. (2016) Shallow burial alteration of dolomite and limestone clumped isotope geochemistry. *Geology* **G37809**, 37801.

Zaarur S., Affek H. P. and Brandon M. T. (2013) A revised calibration of the clumped isotope thermometer. *Earth Planet. Sci. Lett.* **382**, 47–57.

Zachos J., Pagani M., Sloan L., Thomas E. and Bilups K. (2001) Trends, rhythms, and aberrations in global climate 65 Ma to present. *Science* **292**, 686–693.

Associate editor: Thomas M. Marchitto